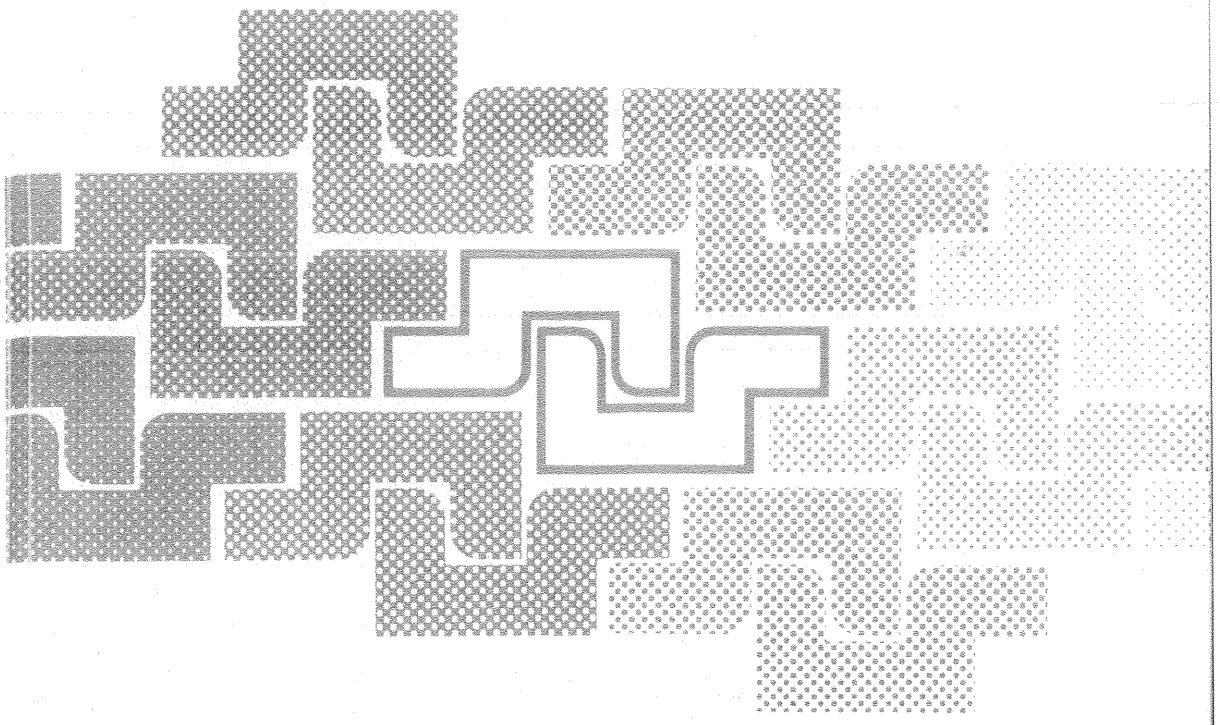

# Beam Shaping and Control with Nonlinear Optics

Edited by
F. Kajzar and
R. Reinisch

NATO ASI Series

Series B: Physics Vol. 369

# INTRODUCTION TO ULTRAFAST AND CUMULATIVE NONLINEAR ABSORPTION AND NONLINEAR REFRACTION

Eric W. Van Stryland

Center for Research and Education in Optics and Lasers, CREOL
University of Central Florida
Orlando, Florida 32816-2700

## INTRODUCTION

We introduce several of the basic processes that lead to third-order nonlinear responses. In general these nonlinearities range from thermally-induced index of refraction changes to the ultrafast bound-electronic nonlinearities of two-photon absorption and its associated nonlinear refraction. While it is relatively easy to distinguish between thermal and ultrafast nonlinearities, there are often ambiguities in single experiments that require careful studies to unravel the basic physical processes. For example, two-photon absorption is easily confused with excited-state absorption where there is a real rather than virtual intermediate state. We give examples of experimental methods to distinguish such processes along with some details of the nonlinear mechanisms. Specifically, we give examples of nonlinear refraction and absorption in semiconductors and wide gap dielectric materials. We introduce the concept of causality and how this relates the absorption and refraction spectra for both linear and nonlinear systems. However, for nonlinear systems, the nondegenerate nonlinearity is needed as obtained, for example, by pump-probe spectroscopy. We also briefly discuss higher-order nonlinearities associated with free carriers (excited states) being generated by two-photon absorption. This leads us to discuss excited-state nonlinearities where the excitation is via linear absorption. These appear as third-order responses but are associated with a cascading of linear susceptibilities, i.e. $\chi^{(1)}{:}\chi^{(1)}$ where $\chi$ is an electric susceptibility. For these nonlinearities it is more convenient to define cross sections than to use the usual expansion in terms of higher-order susceptibilities. If a $\chi^{(3)}$ is defined for a cumulative nonlinearity, it will not be a material constant but will depend on the illumination parameters such as the laser pulsewidth. We go on to look at two-beam interactions which can lead to interesting phenomena such as "weak-wave retardation" and two-beam coupling whose description is useful for the understanding of nonlinear light scattering.

*Beam Shaping and Control with Nonlinear Optics*
Edited by Kajzar and Reinisch, Plenum Press, New York, 1998

## "THIRD-ORDER" NONLINEARITIES

The textbook derivation of nonlinear optics takes the wave equation;

$$\nabla^2\vec{E} - \frac{1}{c^2}\frac{\partial^2\vec{E}}{\partial t^2} = \mu_0\frac{\partial^2\vec{P}}{\partial t^2} \quad , \tag{1}$$

describing the interaction of light with matter through the polarization driving term and expands the polarization P in a Taylor series in the electric field E. Ignoring the vector nature of P and E, nonlocality, the tensorial nature of the susceptibilities and the spatial z dependence, this expansion is;[1]

$$\begin{aligned} P(t) = \varepsilon_0 \int_{-\infty}^{\infty} \chi^{(1)}(t-t_1)E(t_1)dt_1 + \int_{-\infty}^{\infty}\int_{-\infty}^{\infty} \chi^{(2)}(t-t_1,t-t_2)E(t_1)E(t_2)dt_1dt_2 \\ + \int_{-\infty}^{\infty}\int_{-\infty}^{\infty}\int_{-\infty}^{\infty} \chi^{(3)}(t-t_1,t-t_2,t-t_3)E(t_1)E(t_2)E(t_3)dt_1dt_2dt_3 + \ldots \end{aligned} \tag{2}$$

where $\chi^{(n)}$ is defined as the nth-order time-dependent response function or time-dependent susceptibility. Here, we take the field as

$$|\vec{E}(t,z)| = \mathrm{Re}\{E(t,z)\exp[i(kz-wt)]\} \tag{3}$$

with $E$ a complex, slowly varying function of time and space, i.e. it contains both amplitude and phase information. As an example, for harmonic generation (second harmonic from $\chi^{(2)}$ or third from $\chi^{(3)}$) the nonlinearity by necessity follows the rapidly varying field. The only material response capable of this is the ultrafast bound-electronic response, i.e. the so-called "instantaneous" response. Self-action effects come from the odd order susceptibilities and can be caused by a variety of nonlinearities with response times from "instantaneous" for bound-electronic NLR in silica fibers, to seconds as for some photochromic effects (e.g. in photodarkening sunglasses).

As is usually done, Eq. 2 is Fourier transformed to give frequency dependent functions. This gives $P(\omega)$. However, for pulsed inputs, as are usually used in nonlinear optics, the electric fields are narrow functions of frequency and they are still allowed to slowly vary in time (the slowly varying envelope approximation).[2] Similarly the polarization is allowed to slowly follow the field envelope. Therefore $P(\omega)$ becomes a slowly varying function of time, $P_\omega(t)$. For a single frequency input at ω, and looking only at self-action, this leads to a slowly varying polarization at ω given by

$$P_\omega(t) = \varepsilon_0\chi(\omega)E(t) = \varepsilon_0\left[\chi^{(1)}(\omega) + \chi^{(3)}(\omega)\frac{|E(t)|^2}{2} + \ldots\right]E(t). \tag{4}$$

There is a also an implied slow variation with propagation direction, z, not explicitly shown. Writing this Fourier transform as a function of t, as done here and elsewhere, can be somewhat confusing. It assumes that changes of the field, and thus polarization, are so

slow that the material response is the same as for a cw input (i.e. delta function in frequency). Here we ignore the degeneracy factors and the tensor and polarization properties of these nonlinearities. Thus, for example, $\chi^{(3)}$ is an effective nonlinear susceptibility.

In order to demonstrate how this nonlinearity leads to nonlinear absorption, NLA, and nonlinear refraction, NLR, we return to the rapidly varying field and polarization, insert this nonlinearity into the wave equation and neglect diffraction effects i.e. $\nabla^2$ is replaced by $\partial^2/\partial z^2$. The neglect of diffraction effects is a very useful approximation that allows the separation of absorptive and refractive effects. It is a good approximation under the conditions that the linear optics depth of focus of the beam ($Z_0=\pi w_0^2/\lambda$) is much greater than the sample thickness L ($w_0$ is the half width at the $1/e^2$ maximum in the irradiance, HW1/e$^2$M), and the input beam profile is unaffected by the phase distortion induced by nonlinear interactions (i.e. the induced phase distortion is much less than $Z_0$/L). This regime is called "external self-action".[3] The wave equation with Eq. 3 keeping only the most rapidly varying terms can then be reduced to[4]

$$\frac{\partial E(z,t)}{\partial z}-\frac{n}{c}\frac{\partial E(z,t)}{\partial t}=i\frac{\omega}{2nc\varepsilon_0}P_\omega(z,t), \tag{5}$$

where the effect of the linear index has been included. Transforming to coordinates traveling with the wave, $\tau=t-zn/c$ and $z'=z$, leads to the simplified equation[4]

$$\frac{\partial E}{\partial z'}=i\frac{\omega}{2n\varepsilon_0 c}P_\omega=i\frac{\omega}{2nc}\left(\chi^{(1)}+\chi^{(3)}\frac{|E|^2}{2}\right)E, \tag{6}$$

where $E$ and $P$ are functions of $z'$ and $\tau$ and we have only included up to third-order responses. Looking at the magnitude and phase of $E$ by defining

$$E=E_0e^{i\phi}, \tag{7}$$

leads to separate equations describing loss (or gain) and phase shifts;

$$\frac{\partial E_0}{\partial z'}=-\frac{\omega}{2nc}\left(\Im m\{\chi^{(1)}\}+\Im m\{\chi^{(3)}\}\frac{E_0^2}{2}\right)E_0 \tag{8}$$

and

$$\frac{\partial \phi}{\partial z}=\frac{\omega}{2nc}\left(\Re e\{\chi^{(1)}\}+\Re e\{\chi^{(3)}\}\frac{E_0^2}{2}\right). \tag{9}$$

Given that the irradiance $I$ is proportional to $E_0^2$, Eqs. 8 and 9 (or 6) clearly show how the real and imaginary parts of $\chi^{(3)}$ lead to irradiance dependent phase shifts and loss respectively.

The "$i$" in Eq. 6 is important. It shows the $\pi/2$ phase shift between polarization and field. Thus, the polarization can be viewed as having a real part which is in phase with the driving electric field leading to a change of field phase, Eq. 9, and an imaginary part which

leads to a change in the field amplitude, Eq. 8, (index and absorption respectively). We return to this point later when we discuss two-beam coupling.

Rewriting Eqs. 8 and 9 in terms of the irradiance, $I$, and considering only the nonlinearly induced phase $\phi$ results in,

$$\frac{dI}{dz'} = -\left[\frac{\omega}{2nc}\Im m\{\chi^{(1)}\}\right]I - \left[\frac{\omega}{n^2c^2\varepsilon_0}\Im m\{\chi^{(3)}\}\right]I^2 = -\alpha I - \beta I^2, \tag{10}$$

and with $k=\omega/c$,

$$\frac{d\phi}{dz'} = k\left[\frac{1}{2n^2c\varepsilon_0}\Re e\{\chi^{(3)}\}\right]I = kn_2 I \quad , \tag{11}$$

where $\beta$ is defined as the two-photon absorption (2PA) coefficient (in m/W) and $n_2$ is defined as the nonlinear refractive index (in $m^2$/W). Two-photon absorption requires the simultaneous absorption of two quanta of energy $\hbar\omega$. Nonlinear refraction associated with this process is known as the bound electronic Kerr effect characterized by $n_2$. In the literature, $n_2$ is often used to discuss everything from thermal and reorientational (eg. for $CS_2$) index changes, to changes in index from saturation of absorption to ultrafast $\chi^{(3)}$ nonlinearities. Here we restrict the use of $n_2$ to describe the ultrafast index change. Gaussian units (esu) are often used for $n_2$, and a useful relation is

$$n_2(esu) = \frac{cn}{40\pi}n_2(SI) \tag{12}$$

where the right hand side is all in MKS units (SI).

The nonlinear optical properties of materials range from the index change due to the ultrafast interaction of light with bound electrons to the index change caused by the relatively slow thermal expansion of a liquid due to linear absorption. The effects caused by these nonlinear interactions with matter range from the reduction of transmittance from increasing absorption with increasing irradiance (e.g. two-photon absorption) to beam spreading from self-defocusing to the ultimate nonlinear interaction of laser-induced damage. The textbook analysis in terms of $\chi$ is most convenient for describing ultrafast responses. It can also be useful for describing nonlinear interactions where the material response time is short compared with the time scales of the experiments, e.g. compared with the laser pulsewidth. An example here is the reorientation of molecules of $CS_2$ leading to self focusing where most often optical pulses are much longer than the ≅2 ps reorientational time. However, it may not be the most convenient way to describe all nonlinear interactions, for example, those we refer to as cumulative nonlinearities, i.e. ones that build up during the pulse and whose response time is longer than, or on the order of, the pulsewidth. Examples here include thermal nonlinearities, better described by the index change with temperature, $dn/dT$, and excited state nonlinearities where the relaxation time of the excited state is longer than the pulsewidth. In the latter case, the use of cross sections is more convenient than the use of electric susceptibilities. These parameters are materials constants, i.e. independent of the irradiation conditions.

We discuss methods for measuring these different nonlinear responses along with convenient ways to describe them. We concentrate on two types of related nonlinear

interactions; bound-electronic and free-carrier or excited-state nonlinearities. We also describe the intrinsic link that exists between nonlinear refraction and nonlinear absorption due to causality. This linkage allows us to write nonlinear Kramers-Kronig relations relating the nonlinear refraction and nonlinear absorption analogous to the relations relating the dispersion of linear refraction to the linear absorption spectrum.

## KRAMERS-KRONIG RELATIONS

Mathematically, the complex response function of any linear, causal system obeys a dispersion relation that relates the real and imaginary parts of the response function via Hilbert transform pairs. In optics, Kramers-Kronig (KK) relations are dispersion relations relating the frequency dependent refraction, $n(\omega)$ to an integral over all frequencies of the absorption $\alpha(\omega)$ and vice-versa. Toll[5] gave an interesting way of viewing the necessity of these dispersion relations as illustrated in Fig. 1. The electric field of an optical pulse in time (a), consisting of a superposition of many frequencies, arrives at an absorbing medium. If one frequency component (b) is completely absorbed we could naively expect that the output should be given by the difference between (a) and (b) as shown in (c). However, this would obviously violate causality since there is an output signal occurring at times before the incident wave train arrives. In order for causality to be satisfied, the absorption

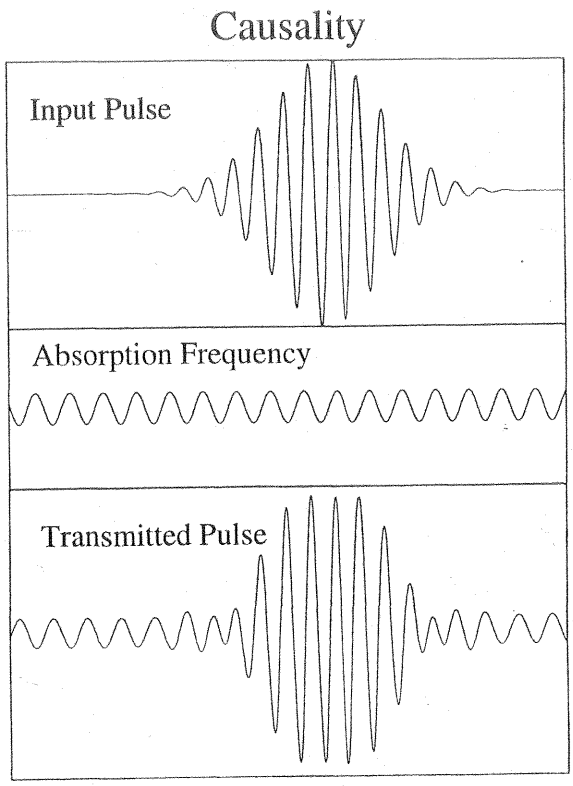


**Figure 1. Illustration of the need for index dispersion.; a) input pulse electric field, b) monochromatic absorption in time, c) "expected" output without dispersion.**

of one frequency component must be accompanied by phase shifts of all of the remaining components in just such a manner that the field prior to the pulse vanishes. Such phase shifts result from the index of refraction and its dispersion.

As will be seen, the real and imaginary parts of $\chi^{(3)}$, or $n_2$ and $\beta$, are related through causality by Kramers-Kronig relations in much the same way as $n$ and $\alpha$ are related for linear optics.[6,7,8,9] This may appear somewhat surprising at first glance since Kramers-Kronig relations are derived from linear response theory. However, we treat the material in the presence of a bright light source as a new "linear" system and then apply causality on this changed system and obtain relations between the changes in absorption, $\Delta\alpha$, and changes in refraction, $\Delta n$. An important difference here with what might first be written for this relation is that the connection is between nondegenerate nonlinearities. That is, the material plus light beam is held constant so that in the integral relation for the nonlinear absorption, it is the change in absorption at frequency $\omega$ due to the presence of a strong beam at $\omega_e$ that is needed; $\Delta\alpha(\omega;\omega_e)$ or $\beta(\omega;\omega_e)$. The above concept is illustrated in Fig. 2. Thus, using this relation requires a knowledge of the spectrum of the nondegenerate nonlinear absorption as obtained, for example, from pump-probe spectra. Therefore, $\Delta n(\omega;\omega_e)$ or $n_2(\omega;\omega_e)$ and $\Delta\alpha(\omega;\omega_e)$ or $\beta(\omega;\omega_e)$ describe the change in refractive index and absorption coefficient, respectively, for a weak optical probe of frequency $\omega$ when a strong pump of fixed frequency $\omega_e$ is applied as illustrated in Fig. 2. The following shows how to mathematically cancel this precursor field in both linear and nonlinear interactions.

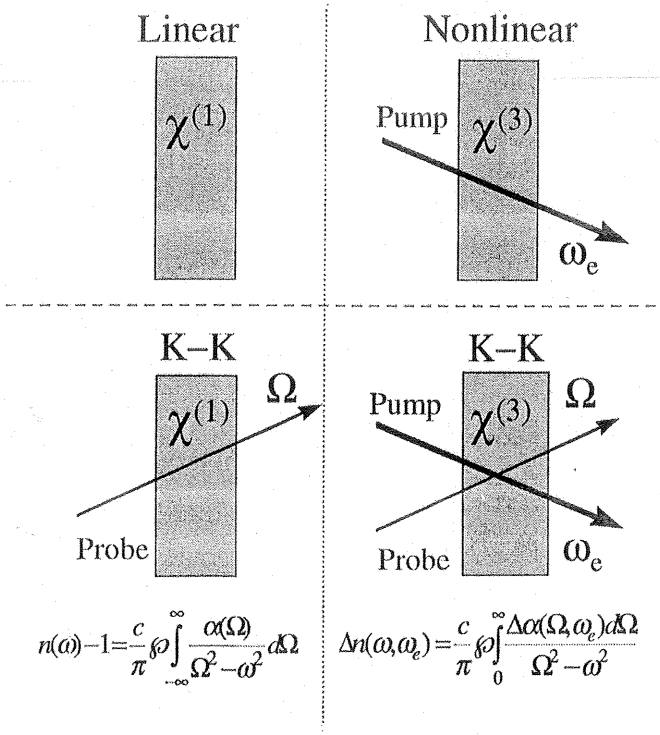


Figure 2. Illustration of Kramers-Kronig relations for linear and nonlinear systems.

## Linear Kramers-Kronig relations

In a dielectric medium the linear optical polarization, P($t$) as given in Eq. 2 is,

$$\mathrm{P}(t) = \varepsilon_0 \int_{-\infty}^{\infty} \chi(\tau)\mathrm{P}(t-\tau)d\tau \,. \tag{13}$$

The response function, $\chi(\tau)$, is equivalent to a Green's function, as it gives the response (polarization) resulting from a delta function input (electric field). This equation is often stated in terms of its Fourier transform, where the convolution in Eq. 13 is transformed into a product

$$P(\omega) = \chi(\omega)E(\omega) \tag{14}$$

where $\chi(\omega)$ is the frequency dependent susceptibility defined by,

$$\chi(\omega) = \int_{-\infty}^{\infty} \chi(\tau)e^{-i\omega\tau}d\tau \,. \tag{15}$$

Causality states that the effect cannot precede the cause requiring that $E(t-\tau)$ cannot contribute to $P(t)$ for $t < (t-\tau)$. Therefore, in order to satisfy causality, $\chi(\tau) = 0$ for $\tau < 0$ so that the integral in Eq. 13 need only be performed for positive times. An easy way to see this is to consider the response to a delta function $\mathrm{E}(\tau) = \mathrm{E}_0\delta(\tau)$, where the polarization would then follow $\chi(t)$. The usual method for deriving the KK relation from this point is to consider a Cauchy integral in the complex frequency plane. However, in the Cauchy integral method, the physical principle from which dispersion relations result (namely causality) is not obvious. The principle of causality can be stated mathematically as

$$\chi(t) = \chi(t)\theta(t) \tag{16}$$

i.e., the response to an impulse at $t = 0$ must be zero for $t < 0$. Here $\Theta(t)$ is the Heaviside step function defined as $\Theta(t) = 1$ for $t > 0$ and $\Theta(t) = 0$ for $t < 0$. Upon Fourier transforming this equation, the product in the time domain becomes a convolution in frequency space

$$\chi(\omega) = \chi(\omega)*\left[\frac{\delta(\omega)}{2} + \frac{1}{2\pi i\omega}\right] = \frac{\chi(\omega)}{2} + \frac{1}{2\pi i}\wp\int_{-\infty}^{\infty}\frac{\chi(\Omega)}{\omega-\Omega}d\Omega = \frac{1}{i\pi}\wp\int_{-\infty}^{\infty}\frac{\chi(\Omega)}{\omega-\Omega}d\Omega, \tag{17}$$

which is the KK relation for the linear optical susceptibility ($\wp$ indicates principle value). Thus, the KK relation is simply a restatement of the causality condition (Eq. 16) in the frequency domain. Taking the real part with $\chi=\chi'+i\chi''$, we have,

$$\chi'(\omega) = \frac{1}{\pi}\wp\int_{-\infty}^{\infty}\frac{\chi''(\Omega)}{\omega-\Omega}d\Omega \,. \tag{18}$$

It is more usual to write the optical dispersion relations in terms of the more familiar quantities of refractive index, $n(\omega)$, and absorption coefficient, $\alpha(\omega)$. These relations are derived in Ref. 8 using relativistic arguments. However, if we assume dilute media with small absorption and indices, we obtain the identical result. By setting $n(\omega)-1=\chi'/2$ and

$\alpha(\omega)=\omega\chi''(\omega)/c$, we obtain

$$n(\omega)-1=\frac{c}{2\pi}\wp\int_{-\infty}^{\infty}\frac{\alpha(\Omega)}{\omega-\Omega}\frac{d\Omega}{\Omega}. \tag{19}$$

Since E($t$) and P($t$) are real, $n(-\omega) = n(\omega)$ and $\alpha(-\omega) = \alpha(\omega)$, which when transforming the integral in Eq. 19 to 0 to $\infty$ gives the final result of

$$n(\omega)-1=\frac{c}{\pi}\wp\int_{0}^{\infty}\frac{\alpha(\Omega)}{\Omega^2-\omega^2}d\Omega\,. \tag{20}$$

**Nonlinear Kramers-Kronig Formalism**

Clearly causality holds for nonlinear systems as well as for linear systems, however, confusion has existed about the application of causality to nonlinear optics. As stated previously, the usual KK relations are derived from linear dispersion theory, so it would appear impossible to apply the same logic to a nonlinear system. The simplest way to view this process is to first linearize the problem by viewing the material plus strong perturbing light beam as a new linear system upon which we apply causality, i.e. the light interaction results in a new absorption spectrum for the material as illustrated in Fig. 2. Thus, both the NLA and the NLR are equivalent to pump-probe spectra with a fixed pump frequency and variable probe frequency.

Here we discuss the Kramers-Kronig relation used to calculate the change in refractive index from the change in third-order absorption. The third-order susceptibility can be determined by integration over positive times only as,

$$\chi^{(3)}(\omega_1,\omega_2,\omega_3)=\int_0^{\infty}d\tau_1\int_0^{\infty}d\tau_2\int_0^{\infty}d\tau_3\,\chi^{(3)}(\tau_1,\tau_2,\tau_3)e^{-i(\omega_1\tau_1+\omega_2\tau_2+\omega_3\tau_3)}. \tag{21}$$

It is now possible to use the same method used earlier for the linear susceptibility in order to derive a dispersion relation for $\chi^{(3)}$. For example, we can write

$$\chi^{(3)}(\tau_1,\tau_2,\tau_3)=\chi^{(3)}(\tau_1,\tau_2,\tau_3)\Theta(\tau_j) \tag{22}$$

where j can refer to any of the three indices and then calculate the Fourier transform of this equation. We could also use two or three step functions, however, the simplest result is obtained by taking just one. This gives us a generalized nonlinear Kramers-Kronig relation for a non-degenerate third-order nonlinear susceptibility (here choosing j=1);

$$\chi^{(3)}(\omega_1+\omega_2+\omega_3:\omega_1,\omega_2,\omega_3)=\frac{-i}{\pi}\wp\int_{-\infty}^{\infty}\frac{\chi^{(3)}(\Omega,\omega_2,\omega_3)}{\omega_1-\Omega}d\Omega\,. \tag{23}$$

This integral is over only one frequency argument, $\Omega$, and all other frequencies are held constant. Thus, we do not obtain a relationship between the degenerate Kerr coefficient, $n_2(\omega)$, and the degenerate two-photon absorption coefficient, $\beta(\omega)$.

Using an analogous definition for the nondegenerate $n_2$ and $\beta$, defined by Eqs. 10 and 11;

$$n_2(\omega;\omega_e)=\frac{1}{n^2c\varepsilon_0}\Re e\{\chi^{(3)}(\omega;-\omega_e,\omega_e,\omega)\} \tag{24}$$

$$\beta(\omega;\omega_e)=\frac{2\omega}{c^2n^2\varepsilon_0}\Im m\{\chi^{(3)}(\omega;-\omega_e,\omega_e,\omega)\}\ . \tag{25}$$

As discussed in Refs. 10 and 11 there is a factor of two difference between the degenerate and nondegenerate definitions. This accounts for cross-modulation or "beating" terms that result for the nondegenerate case for nonlinearities that can respond fast enough. This is sometimes referred to as "weak -wave retardation" as discussed later in this chapter.[12,13] The definition of the nondegenerate $\beta$ now includes all possible nonlinear mechanisms including 2PA, Raman and AC-Stark effects as discussed later in the next section and in Ref. 7.

We can relate these quantities by choosing $\omega_1 = -\omega_2$ with $\omega_2 = \omega_e$ to be the perturbing field frequency (or excitation field) in Eq. 23 and convert to an integral from 0 to $\infty$ to give

$$\mathrm{Re}\{\chi^{(3)}(\omega;\omega_e,-\omega_e,\omega)\}=\frac{2}{\pi}\wp\int_{-\infty}^{\infty}\frac{\Omega\Im m\{\chi^{(3)}(\Omega;-\omega_e,\omega_e,\omega)}{\Omega^2-\omega^2}d\Omega\,. \tag{26}$$

which with the definitions of Eqs. 24 and 25 leads to

$$n_2(\omega;\omega_e)=\frac{c}{\pi}\wp\int_0^{\infty}\frac{\beta(\Omega;\omega_e)}{\Omega^2-\omega^2}d\Omega\,. \tag{27}$$

Although the calculation as illustrated above gives the nondegenerate NLR for a specific pair of frequencies, in most cases we set $\omega=\omega_e$ (after the integral is performed) and consider self-refraction. This gives two times the degenerate nonlinear refractive index $n_2$ (the factor of two difference from weak-wave retardation).

The origin of the nonlinearity need not be optical but of any external perturbation. For example this method has been used to calculate the refractive index change resulting from an excited electron-hole plasma and a thermal shift of the band edge. For cases where an electron-hole plasma is injected, the subsequent change of absorption gives the plasma contribution to the refractive index. In such cases, the excitation in Eq. 27 is not necessarily an optical frequency but can be taken as a general excitation. Thus, $\omega_e$ can represent, for example, the sample temperature change. For nonlinearities due to an existing plasma, $\omega_e$ is taken as the change in plasma density. Van Vechten and Aspnes[14] obtained the low frequency limit of $n_2$ from a similar KK transformation of the Franz-Keldysh electro-absorption effect where, in this case, $\omega_e$ is the DC field. It is important to note that we must first perform the integral before setting $\omega=\omega_e$. This has been a source of confusion in considering saturation of a two-level atomic system as discussed below.

This form of calculation of the refractive index for nonlinear optics is often more useful than the analogous linear optics relation since absorption changes (which can be either calculated or measured) usually occur only over a limited frequency range and, thus, the integral in Eq. 27 need only be calculated over this finite frequency range. In comparison, for the linear KK calculation, absorption spectra tend to cover a very large frequency range and it is necessary to take account of this full range in order to obtain a quantitative fit for the dispersion. For both linear and nonlinear systems the refractive index

changes are usually quite extensive in frequency. Therefore, a calculation of absorption changes from refractive index changes is seldom performed.

**Example: Two-Level Atom**

The familiar saturable "two-level atom" problem is illustrative of the application of the nonlinear Kramers-Kronig relation. The absorption spectrum is given by;[2,15]

$$\alpha(\omega) = \alpha_0 \frac{\gamma^2}{(\omega-\omega_0)^2+\gamma^2} \frac{1}{1+\frac{I}{I_s}\frac{\gamma^2}{(\omega-\omega_0)^2+\gamma^2}} = \alpha_0 \frac{\gamma^2}{(\omega-\omega_0)^2+\gamma^2(1+I/I_s)}, \tag{28}$$

As noted, for example in Yariv's text [15], this does not obey causality. The problem is that as $\omega$ is tuned the excitation is tuned, and the saturation changed for this degenerate form of the absorption. What is needed is the nondegenerate, or pump-probe, absorption spectrum;

$$\alpha(\omega) = \alpha_0 \frac{\gamma^2}{(\omega-\omega_0)^2+\gamma^2} \frac{1}{1+\frac{I}{I_S}\frac{\gamma^2}{(\omega_e-\omega_0)^2+\gamma^2}} = \alpha_0(\omega) \frac{1}{1+\frac{I}{I_S}\frac{\gamma^2}{(\omega_e-\omega_0)^2+\gamma^2}}. \tag{29}$$

Here $\omega_e$ is fixed and $\alpha$ clearly obeys causality since now the absorption spectrum is identical in shape to the linear absorption but simply reduced in amplitude by homogeneous saturation. (Note that we have ignored population pulsations and other more exotic effects in this oversimplified description of the 2-level atom).[2] We next present experimental data and methods for determining the nonlinear coefficients in semiconductors.

## ULTRAFAST NONLINEARITIES IN SEMICONDUCTORS AND DIELECTRICS

The nonlinear optical properties of semiconductors are used for a variety of applications (e.g. optical switching and short pulse production). Some of the largest nonlinearities ever reported have been in semiconductors and involve near-gap excitation. Unfortunately, these resonant nonlinearities, by their nature, involve significant linear absorption. Here we discuss the nonlinear response in the transparency range, i.e. for photon energies far enough below the band-gap energy $E_g$ that bound-electronic nonlinearities either dominate the nonlinear response or are responsible for initiating free-carrier nonlinearities (e.g. two-photon absorption created free carrier nonlinearities). The bound-electronic nonlinearities due to the anharmonic response of bound, valence electrons have been extensively studied in the past [16,7]. The response time for these nonlinearities has been estimated as on the order of 1 femtosecond or less. This ultrafast response time has been exploited in applications such as soliton propagation in glass fibers and recently in the generation of femtosecond pulses in solid-state lasers (Kerr-lens mode-locking). Another significant application is the development of ultrafast all-optical-switching (AOS) devices.

Our interest here is to utilize the Kramers-Kronig relations to determine the dispersion of the bound-electronic $n_2$ from the spectrum of nondegenerate nonlinear absorption. We begin by looking at semiconductor nonlinearities. However, we will find that this also provides a good description of nonlinearities in wide-gap dielectrics. In the transparency range for photon energies greater than half the bandgap energy (i.e. $E_g/2 \le \hbar\omega \le E_g$), two-photon absorption (2PA) dominates the nonlinear losses.[17,18] In a similar way, three-photon absorption (3PA) should dominate for $E_g/3 \le \hbar\omega \le E_g/2$. Other nonlinearities, usually optical damage, make it difficult to observe four-photon absorption and higher nonlinear absorption. Wherrett[19] has shown via second-order perturbation theory for the 2PA transition rate using only one dipole allowed with one dipole forbidden transition with two parabolic bands, that the 2PA scales as $E_g^{-3}$. The forbidden transition (as shown in Fig. 3) is what is referred to as a self transition either within the valence band or within the conduction band that essentially couples the s-like part of the wave function to the p-like part. For semiconductors this coupling depends on the electron or hole momentum, $\kappa$, going to zero at $\kappa=0$. Third-order perturbation theory for allowed-allowed-allowed transitions shows that 3PA scales as $E_g^{-7}$. The identical result for 2PA was obtained using a Keldysh tunneling model by Brandi et. al.[20]

The traditional theoretical approach for calculating $n_2$ and $\beta$ involves direct quantum mechanical calculation of the complex $\chi^{(3)}$ using second-order perturbation theory. Another approach, more suited for absorptive processes, uses transition rate calculations to arrive at $\beta$ via diagrams as in Fig. 3. In order to calculate the nonlinear refraction, we must perform a Kramers-Kronig integral of the nondegenerate nonlinear absorption over all frequencies. This integral, therefore, includes frequencies above the bandgap where linear absorption is possible. In this situation two nonlinear absorption processes in addition to two-photon

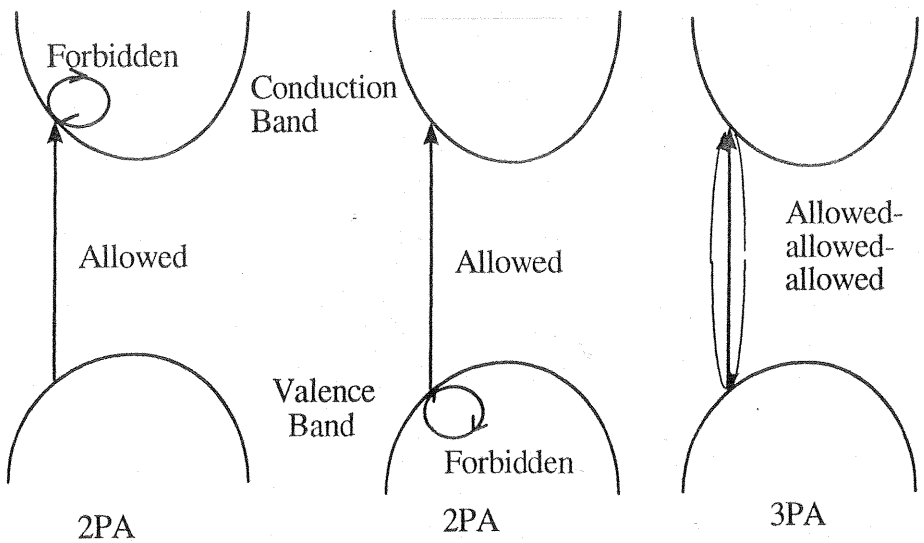


Figure 3. The two-parabolic-band model of a semiconductor showing an allowed followed by a forbidden transition (left) and a forbidden followed by an allowed transition (middle), promoting an electron from the valence to the conduction band via two-photon absorption. The drawing on the right depicts three-photon absorption via an allowed-allowed-allowed transition.

absorption become possible, electronic Raman and the AC-stark effects. Both of these phenomena contribute significantly to the overall nonlinear refractive index. These processes are most easily modeled by using a Keldysh tunneling type model with a "dressed" final state and only keeping the first-order perturbation term in the expansion.[21] Using a two-parabolic band model for the semiconductor, this method gives identical results to second-order perturbation theory for 2PA as given by Wherrett[19] in the degenerate case, but includes these extra nonlinear absorption contributions and directly gives the nondegenerate results as well. Calculations of the nondegenerate nonlinear absorption in the two-parabolic bad model are given in Ref. 22. Both methods give the same scaling of nonlinear absorption with linear index and bandgap energy. In addition, the scaling for $n_2$ is also obtained either from the Kramers-Kronig integral or from the scaling of $\chi^{(3)}$ in the two-band model as given below.

An important goal of nonlinear optical materials characterization is to determine trends from which scaling laws can be developed to give a predictive capability and check theories. After experiments (to be discussed) have been carefully performed and analyzed to extract $\beta$ and $n_2$, we can compare the results to theory. It would be best to make this comparison with the nonlinear spectra for a given material. Unfortunately there are few materials for which nonlinear spectra are known. One reason for this is that tunable sources with the required irradiance, pulsewidth and beam quality are not typically available. Instead we use simple scaling relations to scale out the material dependence. Wherrett[19] has shown that the third-order nonlinear susceptibility, $\chi^{(3)}$, in inorganic solids should scale as

$$\chi^{(3)} \approx \frac{1}{E_g^4} f(\hbar\omega / E_g), \tag{30}$$

where the complex function $f$ depends only on the ratio $\hbar\omega/E_g$ (i.e. upon which states are optically coupled). This yields;

$$\beta(\hbar\omega/E_g) \propto \frac{\hbar\omega}{E_g^4}\mathrm{Im}\{\chi^{(3)}\} \propto \frac{1}{n^2E_g^3}\frac{\hbar\omega}{E_g}\mathrm{Im}\{f(\hbar\omega/E_g)\} \propto \frac{1}{n^2E_g^3}F(\hbar\omega/E_g) \tag{31}$$

$$n_2(\hbar\omega/E_g) \propto \frac{1}{n^2}\mathrm{Re}\{\chi^{(3)}\} \propto \frac{1}{n^2E_g^4}\mathrm{Re}\{f(\hbar\omega/E_g)\} \propto \frac{1}{n^2E_g^4}G(\hbar\omega/E_g) \tag{32}$$

where the defined functions $F$ and $G$ are band structure dependent. Therefore, $F$ gives the 2PA spectrum and $G$ gives the dispersion of $n_2$. One method to test the above scaling relations is to scale the experimental data to obtain the experimental functions (designated by the superscript e);

$$F^e(\hbar\omega / E_g) = \frac{1}{K\sqrt{E_p}}n^2E_g^3\beta^e \tag{33}$$

$$G^e(\hbar\omega/E_g) = \frac{1}{K'\sqrt{E_p}}n^2E_g^4n_2^e \tag{34}$$

where $\beta^e$ and $n_2^e$ are experimental values of $\beta$ and $n_2$, and $K$ and $K'$ are proportionality constants. Here $E_p$ is the Kane energy and is nearly material independent with a value near

21 eV.[23] Figure 4 plots the scaled data for $\beta$ as a function of $\hbar\omega/E_g$, with the predicted dependence from the two-parabolic band model given from perturbation theory or the Keldysh tunneling model. The value of $K$ is fit to the data shown for medium gap semiconductors and has the value $K$=3100 in units so that $E_p$ and $E_g$ are in eV and $\beta$ is in cm/GW and K' comes directly frm the Kramers-Kronig integration (see Eq. 36).[18,8] Figure 4 shows 2PA turning on sharply at half the band-gap energy (there are many data below $E_g/2$ with $\beta \cong 0$ not shown) and then slowly decreasing for photon energies approaching the band gap. While this data is for degenerate 2PA, the theory for nondegenerate 2PA has a similar shape but turns on at $\hbar(\omega_1+\omega_2)=E_g$. The functional dependence of the nondegenerate 2PA is given by,

$$F(x_1,x_2)=\frac{(x_1+x_2-1)^{3/2}}{2^7 x_1 x_2^2}\left(\frac{1}{x_1}+\frac{1}{x_2}\right)^2, \qquad (35)$$

where $x_{1,2}=\hbar\omega_{1,2}/E_g$. Once this functional dependence is known, the extent of variation of the magnitude of $\beta$ can better be seen in a log-log plot of $\beta$ scaled by the spectral response function $F(x_1=x_2)$ versus $E_g$ as in Fig. 5. Here data for other materials including wide gap dielectric materials are included.

With the inclusion of Raman and AC-Stark contribution to the NLA in Eq. 35, we can perform the Kramers-Kronig integral and obtain the dispersion of the nondegenerate NLR. This calculation, in agreement with the scaling relation of Eq. 32 yields for $n_2$ [8]

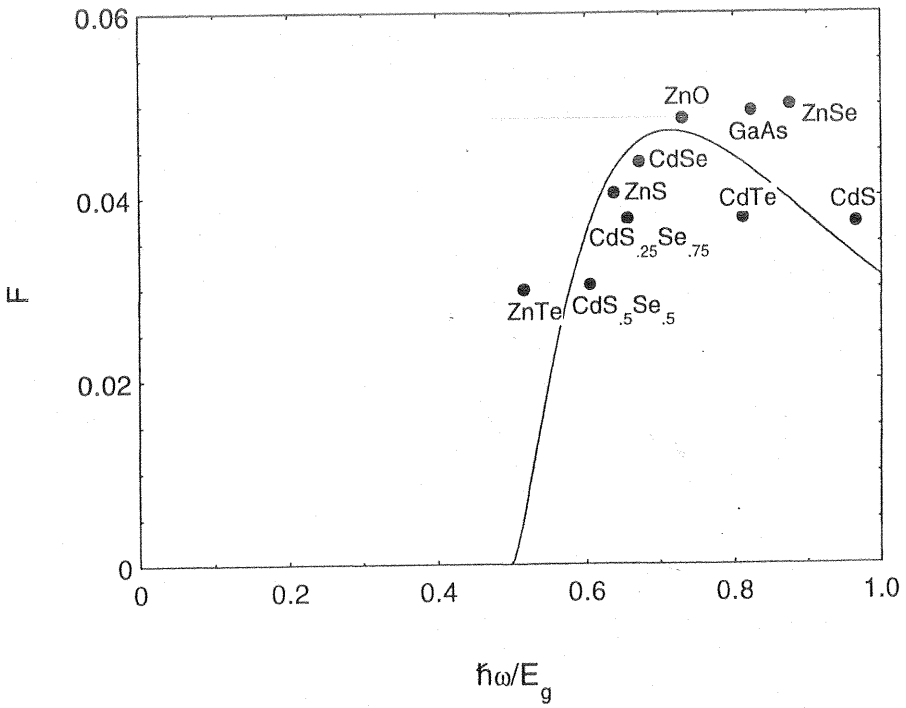


**Figure 4. Scaled values of $\beta$ (according to Eq. 33) as a function of $\hbar\omega/E_g$ along with the theoretical plot of the function $F$ (see Eq. 35 with $x_1=x_2$). Data from Ref. 18.**

$$n_2 = \frac{\hbar cK}{2}\frac{\sqrt{E_p}}{n^2 E_g^4} G(x_1, x_1), \tag{36}$$

while the nondegenerate dispersion function $G$ is given by

$$G(x_1, x_2) = \frac{2}{\pi}\int_0^\infty \frac{F(x'; x_2)}{x'^2 - x_1^2} dx' \quad . \tag{37}$$

Scaling the data as in Eq. 34 ($\omega_1 = \omega_2$) gives the plot of Fig. 6 showing a small, positive, nearly dispersionless $n_2$ for $\hbar\omega/E_g$ much less than $E_g$, reaching a peak near $E_g/2$ (where 2PA turns on) and then decreasing, reaching negative values as $\hbar\omega$ approaches the band edge. The curve is the result of the Kramers-Kronig integral of Eq. 27. This curve is similar to the behavior of the linear index in a solid which has its peak value at the band edge, where linear absorption turns on, and then rapidly turning down toward smaller values as $\hbar\omega$ increases. Note that in order to obtain the degenerate $n_2$, we set $\omega_1 = \omega_2 = \omega$ and divide the result by two to account for "weak-wave retardation".

Again, a large variation in the magnitude of $n_2$, including a change in sign, is hidden by this scaling and is better seen in a log-log plot of $n_2$ scaled by the dispersion function $G$ as given in Fig. 7. At the same time it shows the hidden $E_g^{-4}$ scaling (see Fig. 6) of the

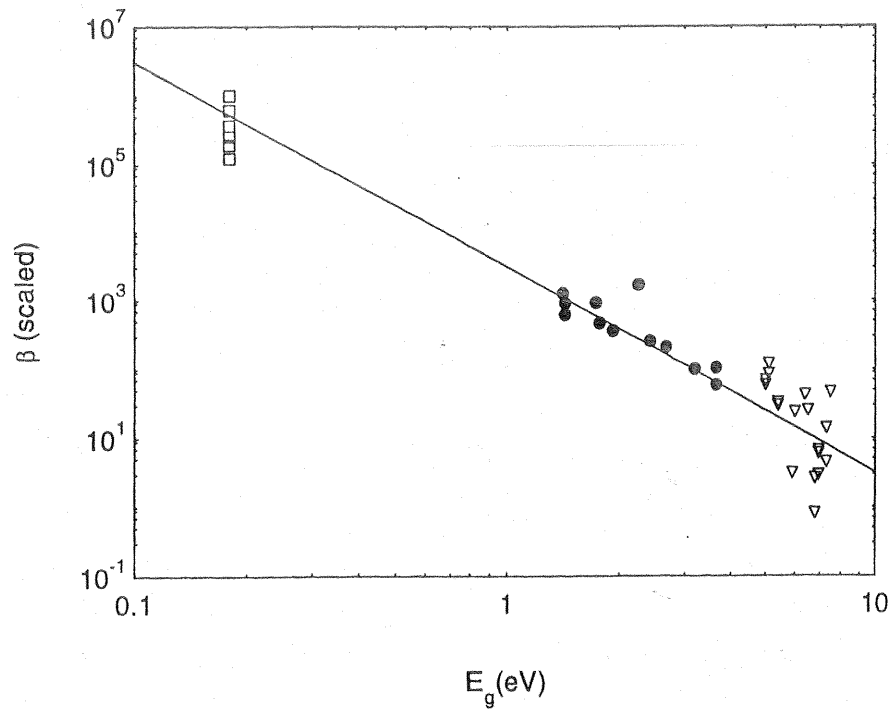


**Figure 5. A log-log plot of scaled data for $\beta$ versus $E_g$ (closed circles from Ref. 18, open triangles form Ref. 24, and open circles for InSb from Ref. 26).**

(36)

(37)

of Fig. 6 showing a small, reaching a peak near $E_g/2$ lues as $\hbar\omega$ approaches the al of Eq. 27. This curve is its peak value at the band own toward smaller values $_2$, we set $\omega_1 = \omega_2 = \omega$ and

a change in sign, is hidden the dispersion function $G$ scaling (see Fig. 6) of the

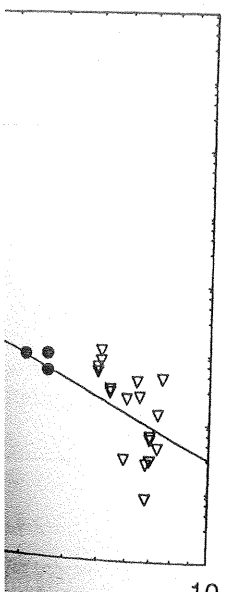


ef. 18, open triangles form Ref.

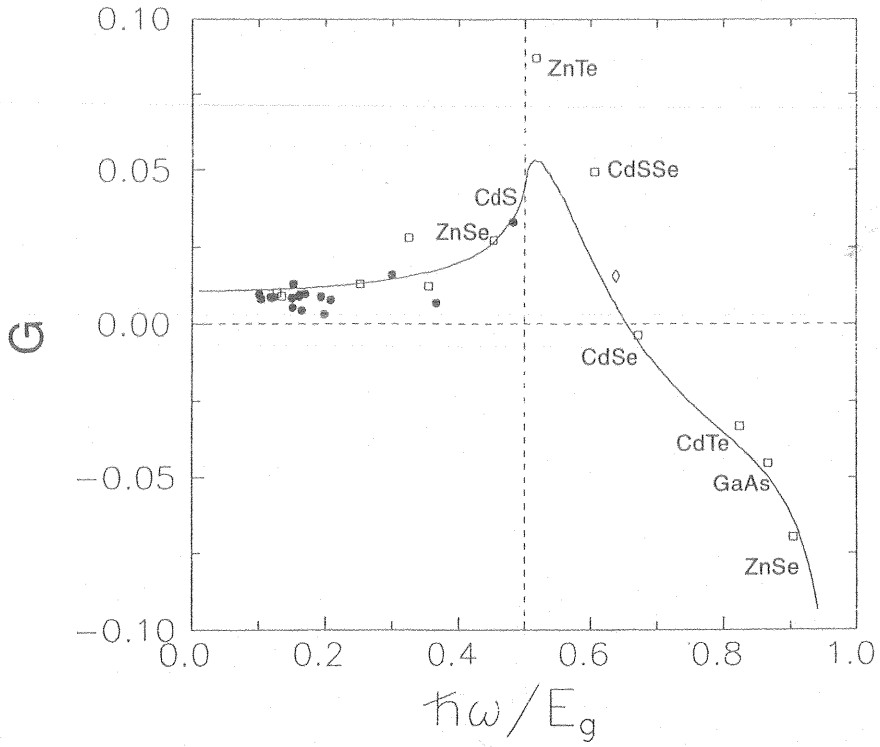


Figure 6. a. A plot of experimental values of the nonlinear refractive index, $n_2^e$, scaled according to Eq. 34 versus $\hbar\omega/E_g$. The solid line is the two-parabolic-band-model prediction for the dispersion function $G_2$. The values for semiconductors (squares) were obtained from Z-scan measurements at 1.06 and 0.532 μm.[7] Also shown are $n_2$ measurements of large-gap optical materials[16] (solid circles). From Ref. 7.

nonlinear index that leads to a wide variation of $n_2$: $2.5\times10^{-14}$ esu for $MgF_2$ at 1.06 μm, $-2\times10^{-9}$ esu for AlGaAs at 810 nm, and $2.7\times10^{-10}$ esu for Ge at 10.6 μm. The straight line is theory showing the $E_g^{-4}$ dependence. It is seen that the scaling law holds over a 5 orders-of-magnitude variation in the modulus of $n_2$. Also note that although the measured values of $n_2$ for ZnSe at 1.06 and 0.532 μm have different signs, both measurements are consistent with the scaling law. More recent data on a series of UV transmitting materials at the harmonics of the Nd:YAG laser are shown in Fig. 8.[25]

We next describe a few of the experimental techniques used to measure $\Delta\alpha$ and $\Delta n$ from which the physical processes can be determined. Adding to the complexity of analysis, Eqs.10 and 11 adequately describe material interactions only when $\beta$ and $n_2$ are solely responsible for the nonlinearity and only when diffraction can be ignored within the material (external self action). As we discuss below, other nonlinear mechanisms must often be included.

## EXPERIMENTAL METHODS

There are a number of difficulties that need to be addressed when attempting to determine the value of $\beta$ or $n_2$ from experiment. An examination of the literature on values of $\beta$ for the semiconductor GaAs show well over a two order of magnitude change in the

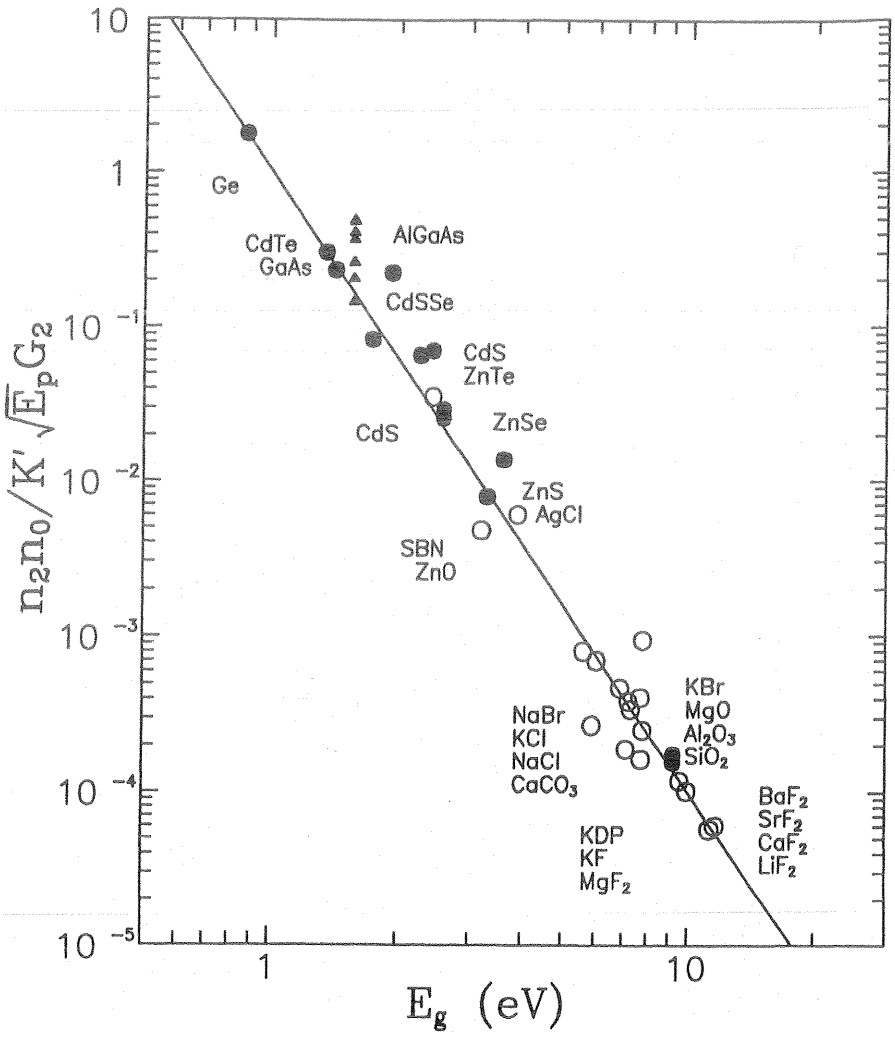


Figure 7. A log-log plot showing the $E_g^4$ dependence of $n_2$. The data points are identical to those in Fig. 6, but are scaled by the dispersion function G. The solid line is the function $E_g^4$ which appears as a straight line of slope –4 on the log-log plot (adapted from Ref. 8).

reported value over the past three decades as shown in Fig. 9. It is illustrative to look briefly at the reasons behind the trend toward smaller values with time shown in this figure. In general the reasons boil down to poorly characterized laser beam parameters and competing nonlinearities, i.e. experimental technique and interpretation. In the early years of these measurements laser pulses were often multimode in either space or time or both, leading to irradiance fluctuations resulting in larger losses from nonlinear absorption than smooth pulsed beams. This leads to an overestimation of $\beta$. More importantly long pulses were used which results in the dominant nonlinear absorption process of free-carrier absorption from the 2PA generated carriers, again resulting in an overestimation of $\beta$ (this is discussed in more detail later under "excited-state nonlinearities). An additional problem is that nonlinear refraction can cause beam size deviation either within the sample or after the sample. If this occurs within the sample the irradiance is changed and, thus the loss is changed. Changes in beam size after the sample can cause errors if some fraction of the

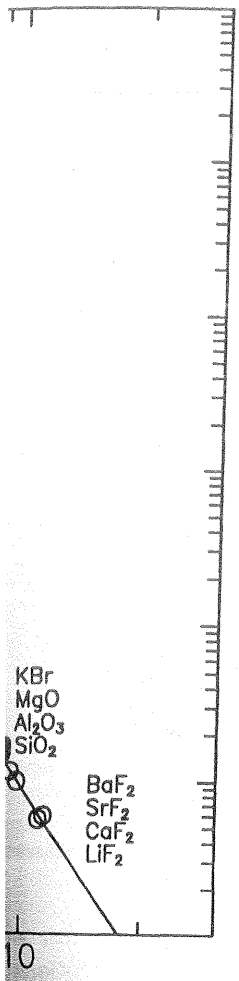


re identical to those in Fig. 6,
which appears as a straight

It is illustrative to look
me shown in this figure.
beam parameters and
ion. In the early years
space or time or both,
nlinear absorption than
portantly long pulses
ess of free-carrier
nation of $\beta$ (this is
itional problem is
mple or after the
thus the loss is
fraction of the

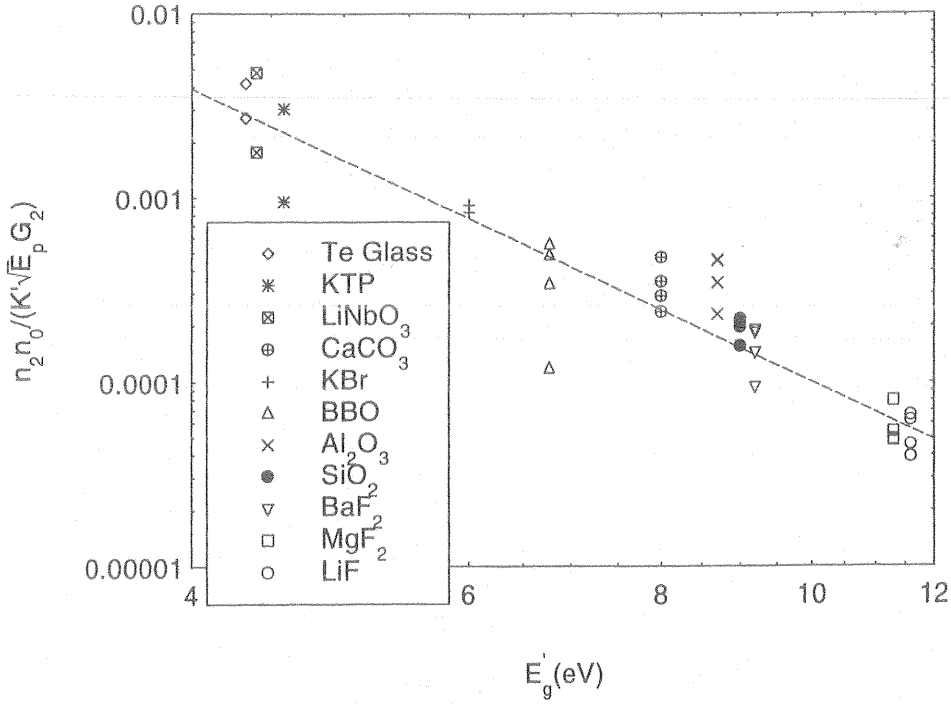


**Figure 8. A similar plot to that of Fig. 7. That is, a log-log plot of $n_2$ data scaled by the dispersion function G versus $\hbar\omega/E_g$ taken with the harmonics of a picosecond Nd:YAG laser on wide bandgap materials. The solid line is the function $E_g^{-4}$ which appears as a straight line of slope –4 on the log-log plot (adapted from Ref. 8)**

transmitted light beam is not collected. This also results in an overestimation of $\beta$. In semiconductors such as GaAs the dominant nonlinear refraction is usually self-defocusing from the 2PA generated carriers. The longer the pulse for a given irradiance the larger the energy and, thus, the greater the carrier density produced and the larger both free-carrier absorption and free-carrier refraction become (see later section on "exited-state nonlinearities.

The solution to the three problems mentioned after they have been identified is relatively simple; use smooth beam profiles, e.g. $TEM_{0,0}$, carefully characterize the output, use short pulses (for most semiconductors 30 ps is short enough to nearly eliminate free-carrier absorption effects, and the carrier defocusing is reduced to a manageable level), carefully collect all the transmitted light (e.g., place a large area detector directly at the back of the sample), and be sure to use samples short enough and irradiance low enough to be in the external self-action regime.

**Beam Propagation**

As an example of beam distortion due to external self-action, Fig. 10 shows the far field energy distribution of a picosecond pulse after transmittance through 2.5 cm of NaCl at low and high irradiance.[27] The curves were normalized to coincide at the center of the beam. The optical path-length change at the center of the beam and at the peak of the pulse due to this bound-electronic $n_2$ as shown in the figure is $\cong\lambda/2.0$. The sensitivity of this method is limited to the order of a $\pi/4$ peak phase distortion with the sample placed at the beam waist of a Gaussian input beam (100 μm $HW1/e^2M$ was used for the data in Fig. 10).

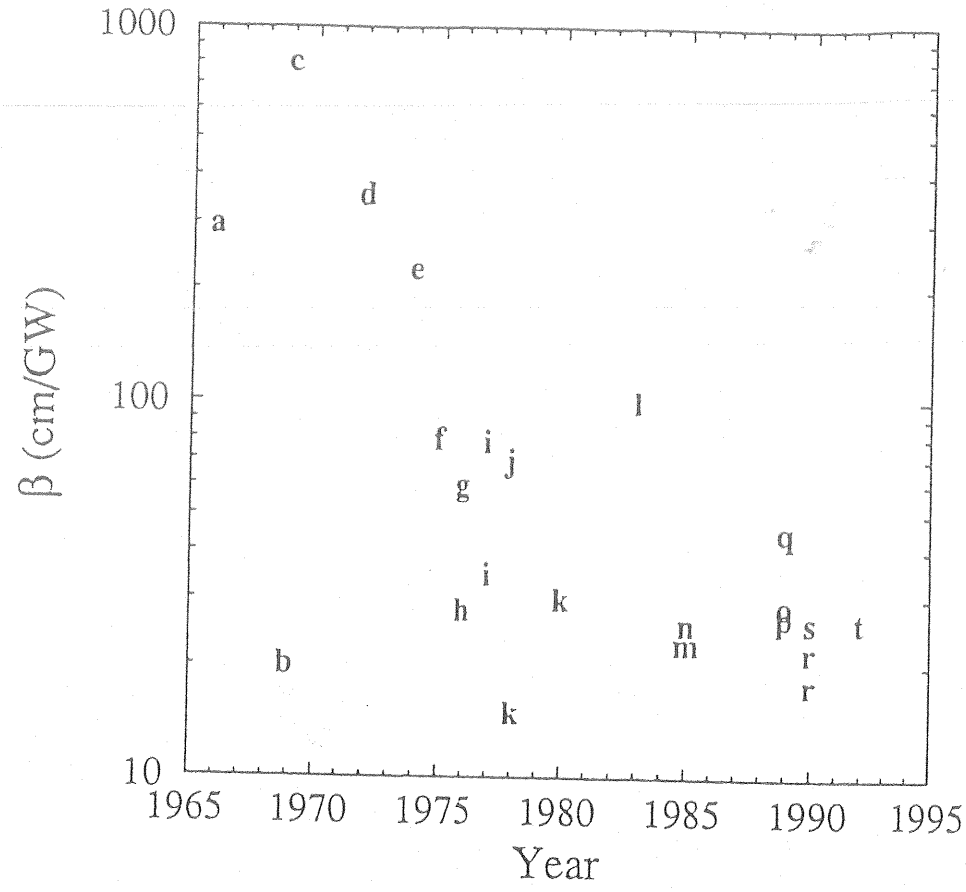


Figure 9. The two-photon absorption coefficient, β, plotted as a function of year published in the literature (note the semilogarithmic scale). The data is from Ref. 26.

However, the sensitivity to induced phase distortion is minimized by placing the sample at the beam waist, i.e. from linear optics, a phase mask or lens has little effect on a beam when placed at the waist. One way to take advantage of the increased effect of a lens on a beam when moved away from the waist is the Z-scan method.

**Z-Scan and EZ-Scan**

We first describe the use of these techniques for measuring NLR. We then describe their use for measuring NLA, and finally describe how NLR can be measured in the presence of NLA. With the development of this method, accurate measurements of $n_2$ in a large number of semiconductors and optical solids in various spectral regions have been obtained.[28,29] The Z-scan has the advantage of easily providing the sign of the nonlinearity, an important factor for the comparison of experiment with theory presented here. Techniques such as degenerate four-wave mixing (DFWM), for example, are sensitive to $|\chi^{(3)}|^2$ so that $\Delta\alpha$ and $\Delta n$ effects are not readily distinguished.

Using a single Gaussian laser beam in a tight focus geometry, as depicted in Fig. 11, we measure the transmittance of a nonlinear medium through a finite aperture (Z-scan) or around an obscuration disk (EZ-scan[30]), both positioned in the far field, as a function of the sample position Z measured with respect to the focal plane. The following example

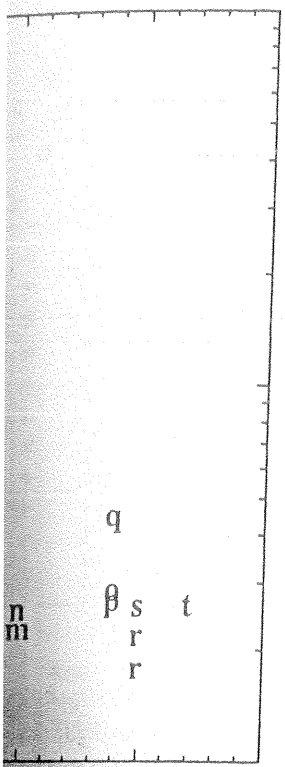


of year published in the literature

ed by placing the sample at
little effect on a beam when
effect of a lens on a beam

NLR. We then describe
be measured in the
measurements of $n_2$ in a
regions have been
sign of the nonlinearity,
theory presented here.
mple, are sensitive to

depicted in Fig. 11,
erture (Z-scan) or
a function of the
lowing example

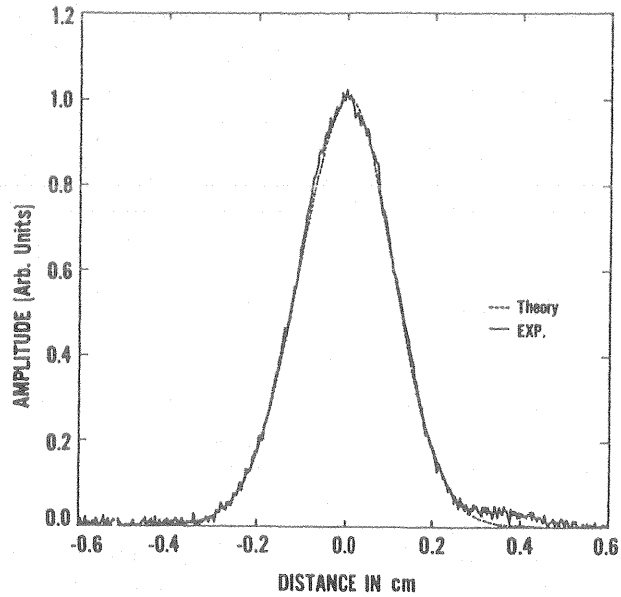


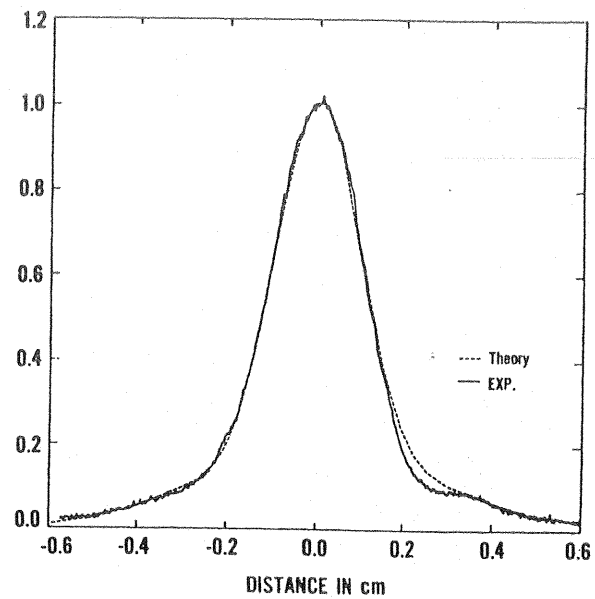


Figure 10. A one dimensional beam scan of a picosecond pulse at 1.06 μm having an initial Gaussian spatial profile after traversing a NaCl sample and propagating to the far field. Left; low irradiance where self-focusing is negligible. Right; high irradiance. From Ref. 27.

qualitatively describes how such data (Z-scan or EZ-scan) are related to the NLR of the sample.

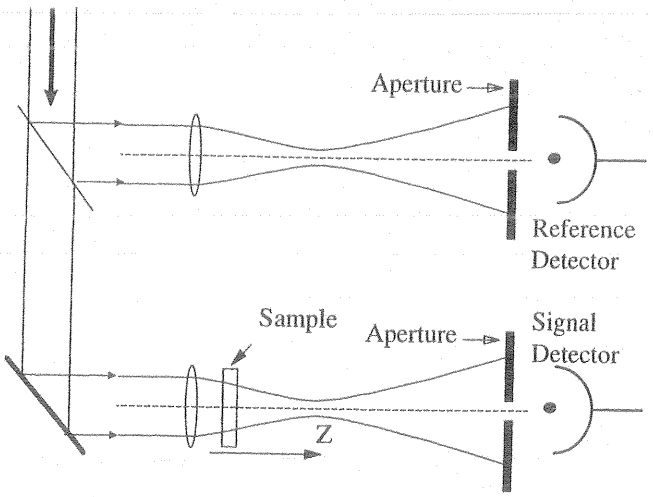


Figure 11. The experimental setup for performing Z-scans (or EZ-scans by replacing the aperture with a disk.

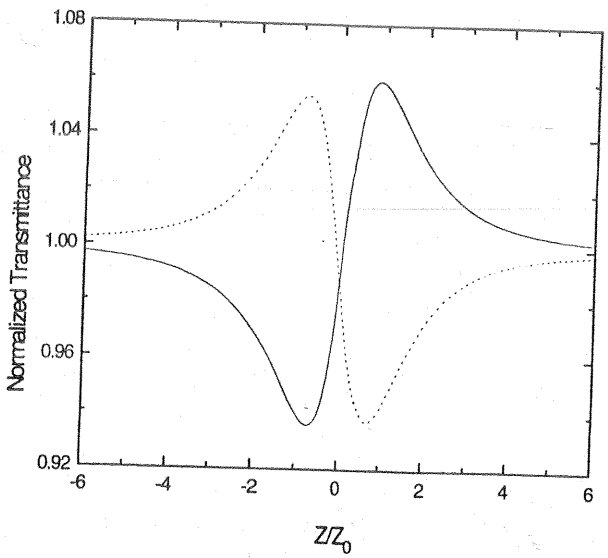


Figure 12. Typical closed aperture Z-scans of a material showing only nonlinear refraction for positive (solid line) and negative (dotted line) $\Delta n$.

Assume, for example, a material with a positive nonlinear refractive index. Starting the scan from a distance far away from the focus (negative Z) the beam irradiance is low and negligible NLR occurs; hence, the transmittance remains relatively constant, and the normalized transmittance is unity as shown in Fig. 12. As the sample is brought closer to focus, the beam irradiance increases leading to self-focusing in the sample. This positive NLR moves the focal point closer to the lens leading to a larger divergence in the far field, thus reducing the transmittance. Moving the sample to behind focus (Z>0), the self-focusing helps to collimate the beam increasing the transmittance of the aperture. Scanning the sample farther toward the detector returns the normalized transmittance to unity. Thus,

related to the NLR of the

Reference Detector

Signal Detector

y replacing the aperture with a

6

refraction for positive

ive index. Starting
m irradiance is low
constant, and the
brought closer to
. This positive
the far field,
>0), the self-
re. Scanning
unity. Thus,

the valley followed by peak signal shown by the solid line in Fig. 12 is indicative of positive NLR, while a peak followed by valley shows self-defocusing.

The EZ-scan can be described in nearly identical terms except we monitor the complementary information of what light leaks past the obscuration disk, or eclipsing disk. Since in the far field, the largest fractional changes in irradiance occur in the wings of a Gaussian beam (see Fig. 10), the EZ-scan can be more than an order-of-magnitude more sensitive than the Z-scan. Figure 13 demonstrates the sensitivity of this method by comparing a Z-scan and an EZ-scan on neat toluene with nanosecond 532 nm pulses under identical experimental parameters (only replacing an aperture by a disk). Note that the vertical scale for the Z-scan is expanded by a factor of 10, and the signal is inverted for the EZ-scan since what is transmitted by an aperture is blocked by a disk. Using this method we have observed a peak optical path length change of as small as $\lambda/2200$ with a signal-to-noise ratio greater than 5 ($\Delta\Phi_0=2\pi/2200$, where $\Delta\Phi_0$ is defined as the integrated peak-on-axis phase shift).[30]

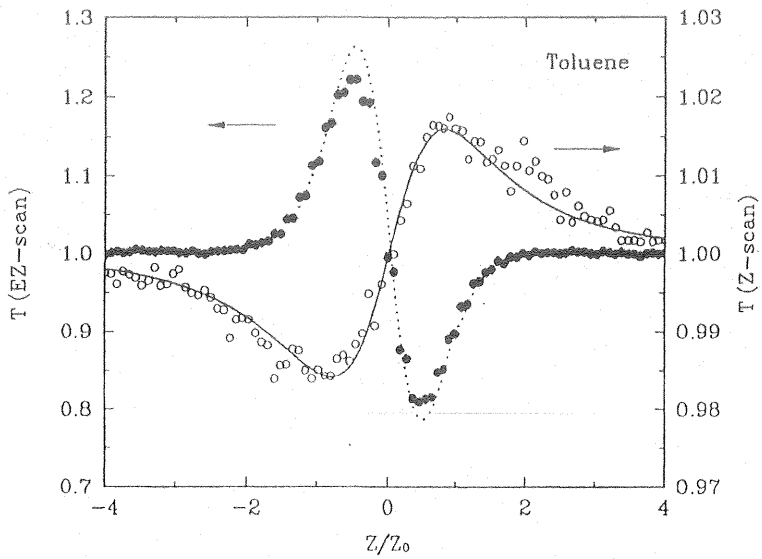


Figure 13. A Z-scan and EZ-scan on toluene. From Ref. 30.

It is an extremely useful feature of the Z-scan (or EZ-scan) method that the sign of the nonlinear index is immediately obvious from the data. In addition the methods are sensitive and simple single beam techniques. We can define an easily measurable quantity $\Delta T_{pv}$ as the difference between the normalized peak and valley transmittance: $T_p$ - $T_v$. The variation of $\Delta T_{pv}$ is found to be linearly dependent on the temporally averaged induced phase distortion, defined here as $\Delta\Phi_0$ (for a bound-electronic $n_2$, $\Delta\Phi_0$ involves a temporal integral of Eq. 11). For example, in a Z-scan using an aperture with a transmittance of $\cong$40%;

$$\Delta T_{pv} \cong 0.36|\Delta\Phi_0| \text{ for } \Delta T_{pv} \leq 1. \tag{38}$$

With experimental apparatus and data acquisition systems capable of resolving transmission changes $\Delta T_{pv}\cong$1%, Z-scan is sensitive to less than $\lambda/225$ wavefront distortion (i.e., $\Delta\Phi_0=2\pi/225$). The Z-scan has a demonstrated sensitivity to a nonlinearly induced optical path length change of nearly $\lambda/10^3$ while the EZ-scan has shown a sensitivity of $\lambda/10^4$.

In the above picture we assumed a purely refractive nonlinearity with no absorptive nonlinearities (such as multiphoton or saturation of absorption). Qualitatively, multiphoton absorption suppresses the peak and enhances the valley, while saturation produces the opposite effect. If NLA and NLR are simultaneously present, a numerical fit to the data can extract both the nonlinear refractive and absorptive coefficients. The NLA leads to a symmetric response about Z=0, while the NLR leads to an asymmetric response (if $\Delta T_{pv}$ is not too large), so that the fitting is unambiguous. In addition, noting that the sensitivity to NLR in a Z-scan is entirely due to the aperture, removal of the aperture completely eliminates the effect. In this case, the Z-scan is only sensitive to NLA. Nonlinear absorption coefficients can be extracted from such "open aperture" experiments. A further division of the apertured Z-scan (referred to as "closed aperture" Z-scan) data by the open aperture Z-scan data gives a curve that for small nonlinearities is purely refractive in nature. In this way we can have separate measurements of the absorptive and refractive nonlinearities without the need of computer fits with the Z-scan. Figure 14 shows such a set of Z- scans for ZnSe. Separation of these effects without numerical fitting for the EZ-scan is more complicated.

The single beam Z-scan can be modified to give nondegenerate nonlinearities by focusing two collinear beams of different frequencies into the material and monitoring only one of the frequencies (different polarizations can be used for degenerate frequencies).[31] This "2-color Z-scan" can separately time resolve NLR and NLA by introducing a temporal delay in the path of one of the input beams. This method is particularly useful to separate the competing effects of ultrafast and cumulative nonlinearities.

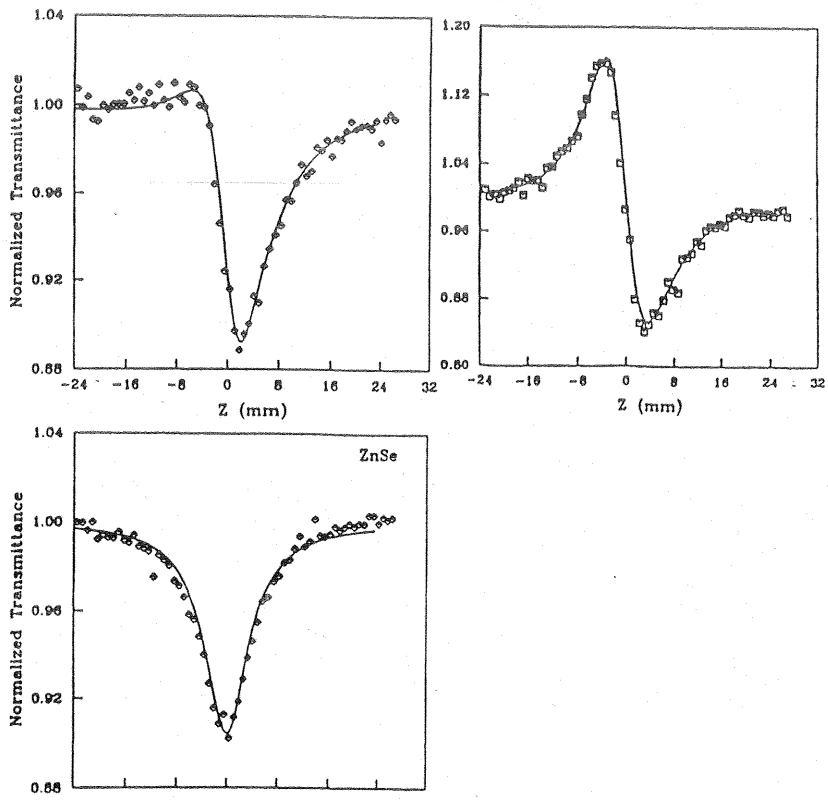


Figure 14. Z-scans of ZnSe showing closed aperture (upper left), open aperture (lower left) and closed divided by open aperture data (upper right). The solid lines are theoretical fits. Adapted from Ref. 7.

## Pump-Probe Z-scan

Pump-probe (or excite-probe) techniques in nonlinear optics have been commonly employed in the past to deduce information that is not accessible with a single beam geometry. The most significant application of such techniques concerns the ultrafast dynamics of the nonlinear optical phenomena. There has been a number of investigations that have used Z-scan in pump-probe scheme. The general geometry is shown in Fig. 15 where collinearly propagating excitation and probe beams are used. After propagation through the sample, the probe beam is then separated and analyzed through the far-field aperture. Due to collinear propagation of the pump (excitation) and probe beams, we are able to separate them only if they differ in wavelength or polarization. The time-resolved studies can be performed in two fashions. In one scheme, Z-scans are performed at various fixed delays between excitation and probe pulses. In the second scheme, the sample position is fixed (e.g. at the peak or the valley positions) while the transmittance of the probe is measured as the delay between the two pulses is varied. The analysis of the 2-color Z-scan is naturally more involved than that of a single beam Z-scan. The measured signal, in addition to being dependent on the parameters discussed for the single beam geometry, will also depend on parameters such as the excite-probe beam waist ratio, pulsewidth ratio and the possible focal separation due to chromatic aberration of the lens. However, these can easily be handled theoretically. Figure 16 shows a temporally-resolved, 2-color Z-scan for ZnSe using 30 ps, 532 nm pulses as the excitation source and 40 ps, 1.064 μm pulses as the temporally delayed probe.[32]

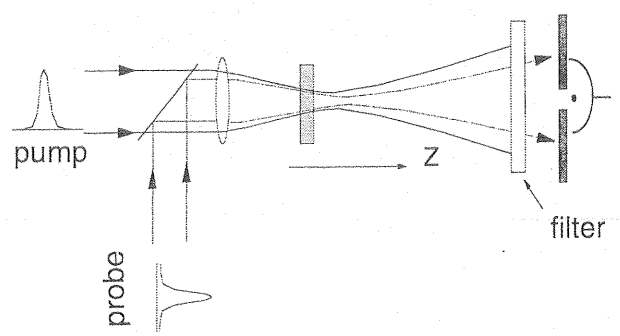


Figure 15. The experimental setup for performing a time-resolved, 2-color Z-scan.

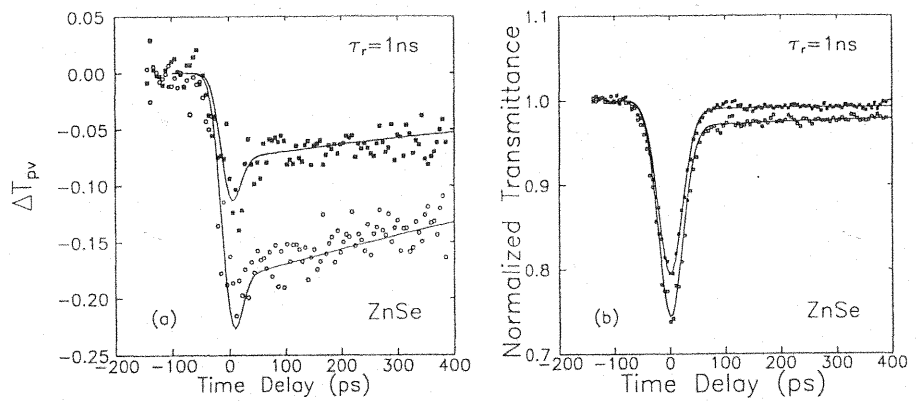


Figure 16. The results of a time-resolved, 2-color Z-scan performed on ZnSe using a 532 nm pump and 1.06 μm probe showing nonlinear refraction vs. time (left) and nonlinear absorption vs. time (right).[32]

## Degenerate Four-Wave Mixing

Another commonly used method to determine the dynamics of the nonlinear response of a material is time-resolved degenerate four-wave mixing (DFWM).[33] One implementation of this technique is shown in Fig. 17 where the interference of the temporally and spatially coincident forward pump (irradiance $I_f$) and probe ($I_p$) sets up a nonlinearity that is examined by the backward pump ($I_b$) as a function of its temporal delay. One interpretation is that $I_f$ and $I_p$ set up a grating whose dynamics is investigated by $I_b$ scattering off this grating into the detector shown in Fig. 17 (often referred to as the "conjugate" direction).[34] While this does not adequately describe the signal within the pulsewidth, it gives a reasonable picture of the longer time response of this method. Figure 18 shows the response in this experiment performed on ZnSe using 30 ps, 532 nm pulses.[35] Clearly there is a fast response following the pulse shape and a slower response with a decay time of 100's of picoseconds (dominated by carrier diffusion washing out the grating). While this technique gives information about the dynamics of the nonlinear response, absorptive and refractive nonlinearities both contribute to the signal and their effects are difficult to separate. That is, in the grating picture, both absorptive and refractive gratings scatter the backward pump into the detector.

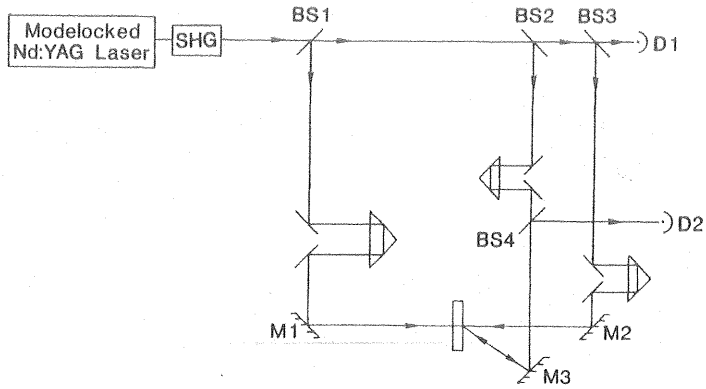


Figure 17. Experimental setup for time-resolved degenerate four-wave mixing (DFWM). From Ref. 35.

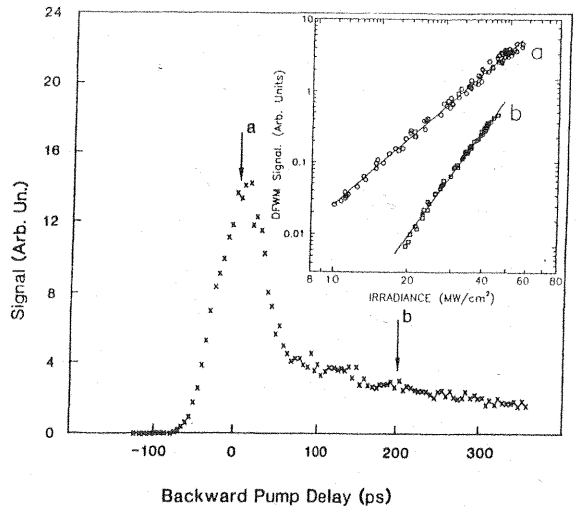


Figure 18. DFWM experiment performed on a sample of ZnSe at 532 nm. From Ref. 35.

namics of the nonlinear
nixing (DFWM).[33] One
the interference of the
and probe ($I_p$) sets up a
ion of its temporal delay.
nics is investigated by $I_b$,
often referred to as the
be the signal within the
e of this method. Figure
30 ps, 532 nm pulses.[35]
slower response with a
fusion washing out the
namics of the nonlinear
to the signal and their
re, both absorptive and

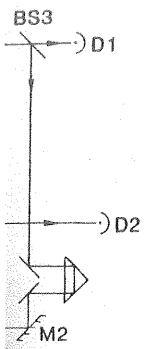


(DFWM). From Ref. 35.

From Ref. 35.

### Streak Camera Imaging

The dynamics of the nonlinear lensing effects can be dramatically demonstrated by monitoring the spatial beam profile in real time with the use of a streak camera. Figure 19 shows the spatial profile at low and high input energies for 30 ps, 532 nm pulses incident on ZnSe after propagation in the relatively near field.[36] At high inputs the 2PA creates carriers which are long lived with respect to the pulsewidth used and build up in time with the integrated energy. Thus, the defocusing from these carriers is observed in Fig. 19 to get stronger with increasing time in the pulse.

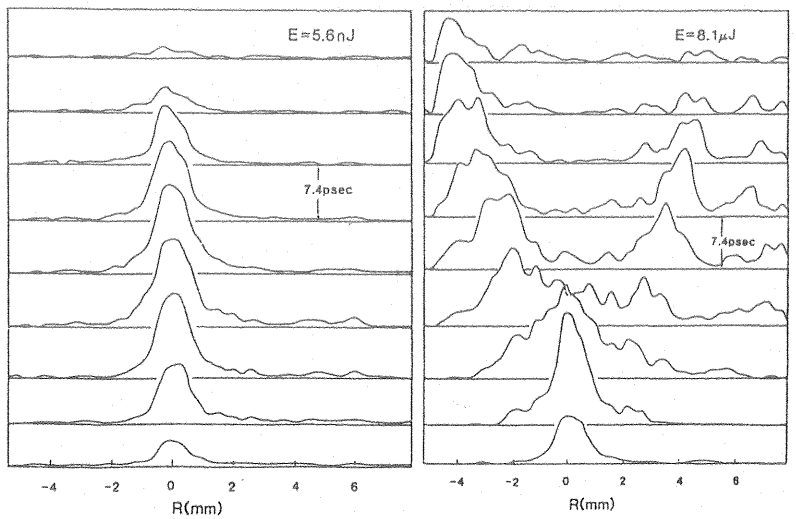


Figure 19. Spatial scans at different times (separated by 7.4 ps) in the pulse after transmission through ZnSe and propagation to the near field as measured using a streak camera/vidicon combination. The left side shows low energy (i.e. the input shape) and the right side shows the defocusing at high input. From Ref. 36.

## EXCITED-STATE NONLINEARITIES

Both Figs. 16 and 18 show a fast response mimicking the input pulse (i.e. a response time less than the input pulsewidth) along with another more slowly responding nonlinearity. The rapid response is either a combination of degenerate 2PA, $\beta(2\omega)$ and $n_2(2\omega)$ effects for the DFWM experiment (see Fig. 18), or the separate effects of nondegenerate 2PA, $\beta(\omega;2\omega)$, for the 2-color Z-scan and nondegenerate $n_2(\omega;2\omega)$, see Fig. 16. Here $\omega$ correspond to a wavelength of 1.064 μm. The longer time response in Figs. 16 and 18 (and 19) is due to the nonlinear absorption and refraction induced by 2PA generated carriers. The generation rate for these carriers of density N is given by

$$\frac{dN}{dt} = \frac{\beta I^2}{2\hbar\omega} . \tag{39}$$

The absorption from these carriers is referred to as free-carrier absorption, FCA, and the refraction as free carrier refraction, FCR and both effects are linear in the carrier density. While the FCA and FCR depend on the carrier density independent of their generation mechanism, when the carriers are generated via 2PA these effects appear as fifth order

nonlinearities or, as an effective, pulsewidth dependent $\chi^{(5)}$.[37] However, they are best described in terms of absorptive ($\sigma_a$) and refractive ($\sigma_r$) cross sections as;

$$\left.\frac{dI}{dz}\right|_{FCA} = -\sigma_a N I$$
$$\left.\frac{d\phi}{dz}\right|_{FCR} = \sigma_r N \qquad (40)$$

Sometimes k is included in the phase equation changing the units of $\sigma_r$ to length cubed. The sign of $\sigma_a$ is intrinsically positive while, in principle $\sigma_r$ can have either sign. In fact, however, for below gap excitation, $\sigma_r$ is always negative leading to self-defocusing. Once excited, these carriers can undergo a variety of processes including several types of recombination and diffusion which have not been included in Eq. 40. For short pulse excitation (e.g. ps) with pulsewidths less than recombination and diffusion times Eq. 39 is adequate to describe the response within the duration of the pulse. Combining the 3rd and 5th order responses gives,

$$\frac{d\phi}{dz} = kn_2 I + k\sigma_r N \ . \qquad (41)$$

The dynamics of these carriers is seen in the time-resolved Z-scan of Fig. 16, the DFWM data of Fig. 18 and the streak camera imaging of Fig. 19. In the Z-scan data carrier recombination dominates the decay while in the DFWM experiment carrier diffusion between peaks and valleys of the grating dominates. These decays would need to be included in Eq. 39 to describe these dynamics. The order of the response is seen in the DFWM data as the inset of Fig. 18 where the signal at two time delays is plotted as a function of the input irradiance I (all three input irradiances varied simultaneously). At zero delay the slope of the signal versus I is three (third-order, $\chi^{(3)}$ response) while at a 200 ps delay (well past the overlap of the pulses), the slope is five indicating the fifth-order response.

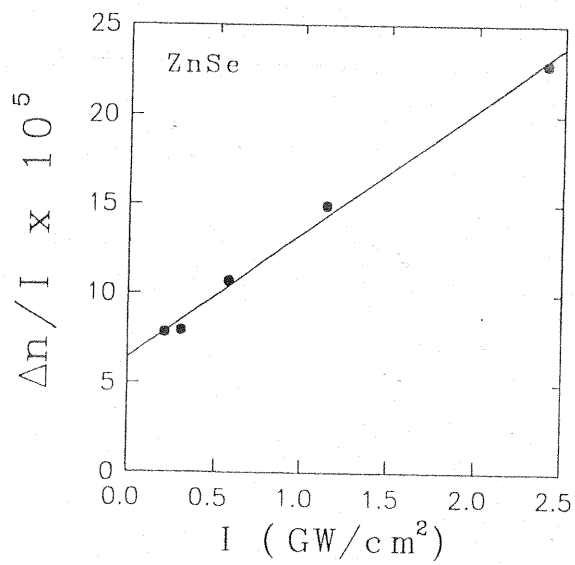


Figure 20. A plot of the index change, Δn, divided by the irradiance, I, as a function of I. From Ref. 37.

This higher-order response for nonlinear refraction is also observed in Z-scans performed at different irradiance inputs of 532 nm picosecond pulses. At low inputs the third-order bound-electronic response dominates while at higher inputs the fifth-order self-defocusing from the 2PA generated free carriers becomes important. Figure 20 shows the index change divided by the peak-on-axis input irradiance, $I_0$, in ZnSe at 532 nm, as a function of $I_0$. The index change is calculated from the measured $\Delta\Phi_0$. For a purely third-order response, $\Delta n = n_2 I_0$, and this figure would show a horizontal line. The slope of the line shown in Fig. 20 shows a fifth-order response while the intercept gives $n_2$, the negative bound-electronic defocusing at 532 nm. This helps explain some of the discrepancies of measured values of 2PA coefficients in GaAs (see Fig. 9). These higher order nonlinearities seen in semiconductors give some indication of the importance of the careful characterization needed to interpret the measured nonlinear loss and phase.

It would seem reasonable that $\sigma_r$ and $\sigma_a$ would be related by causality through Kramers-Kronig relations. However, after excitation there can be rapid redistribution of the carriers within the bands due to various mechanisms. This redistribution leads to so-called band-filling nonlinearities, and for the time scales of picoseconds used in the experiments shown, this prohibits the use of Kramers-Kronig relations for the cross sections (note that after excitation and redistribution the absorption and refraction due to these carriers are related by Kramers-Kronig relations).

## EXCITED-STATE NONLINEARITIES VIA ONE-PHOTON ABSORPTION

As discussed in the previous section, excited carriers can lead to NLA and NLR. In other materials such as molecular systems, the creation of excited states can lead to analogous nonlinearities described by identical equations (Eqs. 40) where N is interpreted as the density of excited states. Again, how they are generated is unimportant. If the carriers or excited states are created by 2PA the resulting nonlinearities are fifth order, i.e., an effective $\chi^{(5)}$. Depending on the absorption spectra, these states can also be created by linear absorption where, neglecting decay within the pulse,

$$\frac{dN}{dt} = \frac{\alpha I}{\hbar\omega}. \tag{42}$$

Concentrating on molecular nonlinearities we refer to these nonlinearities as excited-state nonlinearities, ESA and ESR in analogy to FCA and FCR respectively. Assuming that depletion of the ground state can be ignored (i.e., no saturation),

$$\frac{dI}{dz'} = -\alpha I - \sigma_a N I . \tag{43}$$

By temporal integration of Eqs. 43 with 42 we find;

$$\frac{dF}{dz'} = -\alpha F - \frac{\alpha\sigma_a}{2\hbar\omega}F^2 \tag{44}$$

where $F$ is the fluence (i.e., energy per unit area). This equation is exactly analogous to Eq. 10 which describes 2PA, except that the irradiance is replaced by the fluence and the 2PA coefficient, $\beta$ is replaced by $\alpha\sigma_a/2\,\omega$. Thus, experiments such as Z-scan will monitor a third-order nonlinear response that could easily be mistaken for 2PA. However, there must be some linear absorption present, however small, for ESA to take place. Two-photon-

absorption does not require linear loss. Unfortunately this is not enough to differentiate the processes as there can be linear absorption present in 2PA materials unrelated to the NLA process, e.g. from impurities or other absorbing levels. A temporally resolved measurement, such as DFWM or time-resolved Z-scan, would also show the excited-state lifetime assuming the pulsewidth was short compared to this lifetime. Another way to determine the mechanism is to measure the nonlinear response for different input pulsewidths, again assuming the pulses can be made shorter than the excited state lifetime. Figure 21 shows this measurement performed on a solution containing chloro-aluminum phthalocyanine (CAP).[38] While the energy in the pulses was held fixed while the irradiance was changed by a factor of two by changing the pulsewidth, the nonlinear transmittance remained the same in the open aperture Z-scans. This clearly indicates that the NLA is fluence rather than irradiance dependent and, therefore, must be described by a real state population, i.e., ESA. In CAP, at 532 nm, the ESA cross section $\sigma_a$ is considerably larger than the ground-state cross section. This type of absorber is referred to as a reverse-saturable absorber since the absorption increases with increasing input. Such effects are useful in optical limiting.[39] For large inputs the ground state can become depleted reducing the overall NLA.

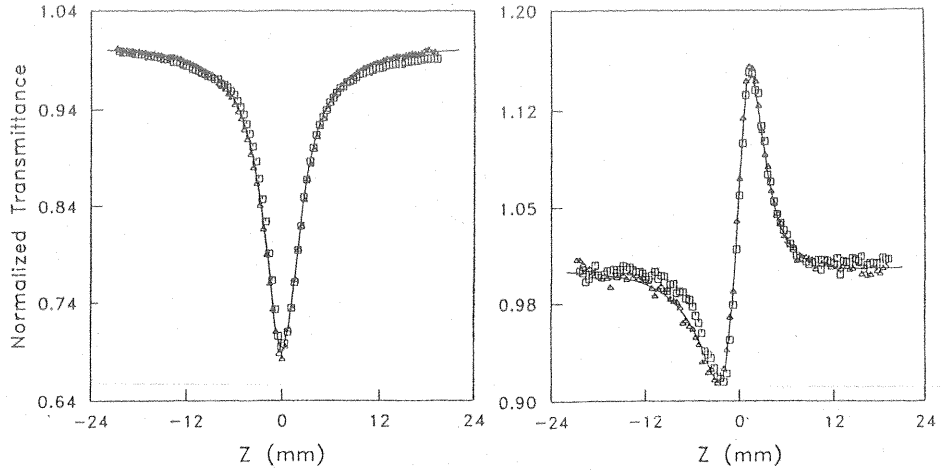


**Figure 21. Z-scans performed on a sample of CAP at 532 nm. The left shows open aperture Z-scans for pulsewidths of 29 ps (squares) and 61 ps (triangles) and the right shows closed aperture Z-scans (after absorption is divided out) for the same pulsewidths. Adapted from Ref. 38.**

Associated with ESA is ESR as given by the second term in Eq. 41, which is simply due to the redistribution of population from ground to excited state. This is analogous to the index change in a laser from gain saturation which leads to frequency pulling of the cavity modes.[2] Ground state absorbers are being removed and excited state absorbers are being added. Depending on the spectral position of the input with respect to the peak linear and peak excited-state absorption, the NLR can be of either sign. For reverse saturable absorbing materials the NLR is most likely controlled by the addition of excited-state absorbers, and their spectrum since the cross section is larger. Thus N is determined by Eq. 42. Figure 21 also shows the NLR in CAP for two different pulsewidths demonstrating that it is also fluence dependent and, thus, dependent on real state populations.

## TWO-BEAM INTERACTIONS

Here we give examples of "nondegenerate" nonlinearities, where here the breaking of degeneracy is not just frequency, but propagation direction, e.g. 2-beam coupling. There

enough to differentiate the
rials unrelated to the NLA
ally resolved measurement,
the excited-state lifetime
other way to determine the
input pulsewidths, again
lifetime. Figure 21 shows
aluminum phthalocyanine
irradiance was changed by
ittance remained the same
LA is fluence rather than
tate population, i.e., ESA.
ger than the ground-state
turable absorber since the
l in optical limiting.[39] For
erall NLA.

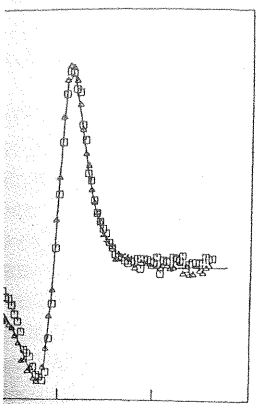


ws open aperture Z-scans for
closed aperture Z-scans (after

n Eq. 41, which is simply
tate. This is analogous to
frequency pulling of the
xcited state absorbers are
respect to the peak linear
gn. For reverse saturable
addition of excited-state
as N is determined by Eq.
widths demonstrating that
ulations.

here here the breaking
beam coupling. There

are many phenomena that can occur when two beams are coincident in space and time on a nonlinear sample. Among these are cross-phase modulation where a pump beam modulates the phase of a probe through the optical Kerr effect, 2PA induced on the probe, excited species created by the pump affecting the probe or temperature changes induced by the pump changing the index seen by the probe. In these cases, if the probing beam, p, is much weaker than the pump (exciting beam e), the changes in the weak probe beam can be twice as large as the changes in the strong beam (the strong beam is unaffected by the weak probe). This factor of two comes from the cross term or grating term in the nonlinear interaction and is sometimes referred to as weak-wave retardation.[12] From Eq. 4 with two input fields $E_e(t,z)\exp[i(\vec{k}_e\cdot\vec{r}-\omega t)$ and $E_p(t,z)\exp[i(\vec{k}_p\cdot\vec{r}-\omega t)$ and keeping only the third-order self-action term (ignoring their vector nature other than keeping track of the wave-vector dependence) gives;

$$P_{NL}=\frac{\varepsilon_0}{2}\chi^{(3)}\left\{|E_e|^2+|E_p|^2+\left(E_eE_p^*e^{i(\vec{k}_e-\vec{k}_p)\cdot\vec{r}}\;E_e^*E_pe^{i(\vec{k}_e-\vec{k}_p)\cdot\vec{r}}\right)\right\}\times\left(E_ee^{i\vec{k}_e\cdot\vec{r}}+E_pe^{i\vec{k}_p\cdot\vec{r}}\right) \tag{45}$$

We plug this equation into the reduced wave equation given in the slowly varying amplitude and phase approximation by Eq. 6. Looking just at the terms with k vectors in the pump $\exp(i\vec{k}_p\cdot\vec{r})$, and probe, $\exp(i\vec{k}_e\cdot\vec{r})$, directions separately, we have;

$$\frac{\partial E_e}{\partial z}=i\frac{\omega}{4cn}\chi^{(3)}|E_e|^2E_e$$
$$\frac{\partial E_p}{\partial z}=i\frac{\omega}{4cn}\chi^{(3)}2|E_e|^2E_p\,, \tag{46}$$

where it has been assumed that $E_p<<E_e$. This explicitly shows the factor of two difference in the nonlinearity seen by the pump and by the weak probe. The $|E|^2$ acts like an irradiance or time averaging of the field squared. This averaging can have important consequences if the nonlinearity has a finite response time compared to the pulsewidth. For example, let's assume that the pump pulse creates excited states that change the index of refraction (or absorption) as seen by the probe pulse. We then write the slowly varying nonlinear polarization at ω for the two beams separately by observing their separate k dependence as;

$$P_e(t)=\varepsilon_0\,"\chi^{(3)}\,"E_e(t)\int_{-\infty}^{t}|E_e(t')|^2e^{-(t-t')/\tau_L}dt'$$
$$P_p(t)=\varepsilon_0\,"\chi^{(3)}\,"\left\{\begin{array}{l}E_p(t)\int_{-\infty}^{t}|E_e(t')|^2e^{-(t-t')/\tau_L}dt'\\+E_e(t)\int_{-\infty}^{t}E_e^*(t')E_p(t')e^{-(t-t')/\tau_G}dt'\end{array}\right\} \tag{47}$$

where $\tau_L$ is the excited-state lifetime and $\tau_G$ is the grating lifetime, both assumed here to have exponential decays. The quotation marks are placed around $\chi^{(3)}$ since this is really describing a $\chi^{(1)}$: $\chi^{(1)}$ effect. The second term in $P_p$ is called the grating term because it arises from the pump scattering off the material grating induced in the sample by the interference of the pump and probe beams. The grating decay is in general shorter than the excited-state decay since it includes the latter but also decays via diffusion which smoothes the grating in time. Note that if the pulsewidth is long compared to the grating decay time but short compared to the excited-state lifetime, the grating term will not contribute significantly to the nonlinearity and the pump and probe will see the same nonlinear response, both seeing only the direct effect of the pump.

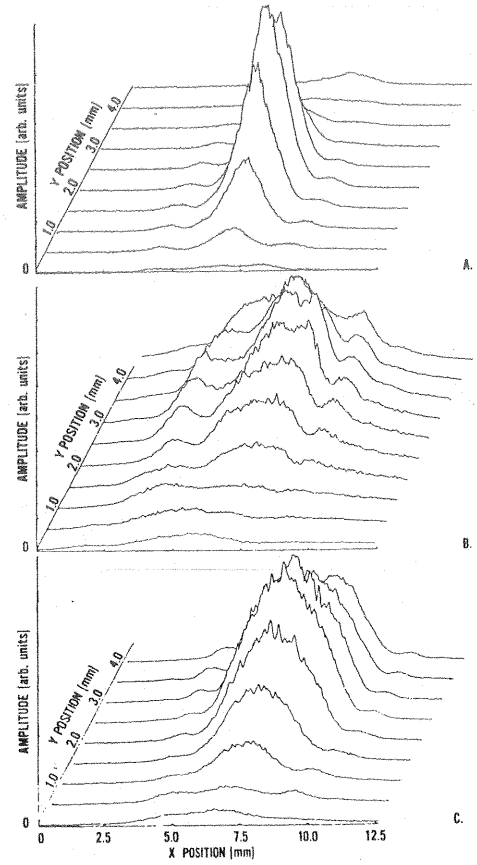


**Figure 22. Vidicon images of the spatial irradiance distribution of an originally Gaussian spatial profile beam after traversing a Si sample and propagating to the far field A) probe without pump, B) probe with pump C) pump beam. From Ref. 12.**

Such a grating can or cannot cause energy to be transferred between the two beams (2-beam energy transfer- or 2-beam coupling) depending on the relative phase of the grating produced with respect to the irradiance modulation. We'll get back to this point later. A very graphic example of this weak-wave retardation can be seen by looking at the self-defocusing produced in silicon by the generation of free-carriers by linear absorption.[12] Once carriers are generated (excited) the index of refraction is lowered (band-blocking). This appears as a third-order nonlinearity ($\chi^{(1)}$:$\chi^{(1)}$ rather than $\chi^{(3)}$). Figure 22 shows the transmitted 1.06 μm beam profiles in the far field after propagating through 270 μm of

silicon. Silicon is an indirect gap semiconductor and 1.06 μm falls below the direct gap but above the indirect gap so that the transmittance for this sample length is ≅25% including Fresnel reflection losses. The 65 ps (FWHM) pulses are short compared to carrier lifetimes and diffusion times assuring that the nonlinearity including the grating did not decay within the pulsewidth so that the nonlinearity accumulates throughout the pulse without decay. As shown in the figure, the weak probe beam undergoes more self-defocusing (more phase distortion) than the excitation beam (≅2x). By temporally delaying the probe with respect to the pump we can see how this nonlinearity builds up from carriers excited by the pump with time as shown in Fig. 23. The scattering of light off the grating is graphically shown by moving the vidicon to the near field as seen in Fig. 24 where both beams can be simultaneously observed. Here the pump and probe pulse have equal energy to show the extra scattered beams on either side of the pump and probe. The beams diffracted in the outer directions are the other order beams (i.e. there is a +1 and -1 order diffraction) in the thin grating region. This thin grating or Raman-Nath limit is appropriate in this experiment where the sample is thin and the angle between beams is small ≅$1.2^0$. The extra beam (when the probe is small) is often called the forward scattered conjugate beam. In the case of silicon, where the primary nonlinear interaction is the index change due to the creation of free carriers (the excited states), there is not a direct transfer of energy from the pump to the probe since the phase of the scattered light is $\pi/2$ out of phase, i.e. an index effect. This $\pi/2$ phase shift is seen as the $i$ in the field change, $\partial E/\partial z$, equations, e.g. see Eq. 46. It indicates that the phase of $E$ is normally changed by Re{$\chi$}. A shift in the phase of the grating can lead to amplitude changes in the probe from Re{$\chi$}. There is, however, energy transferred to the forward conjugate beams since in these directions there is no light to "interfere" with. We discuss energy transfer or 2-beam coupling more in what follows.

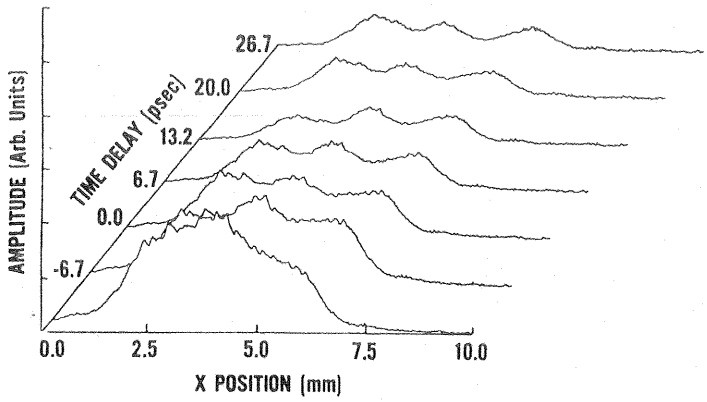


**Figure 23. The spatial profile of the probe beam of Fig. 22B as a function of the time delay between the pump and probe.**

In order to have energy transferred, the phase term in the $\partial E/\partial z$ equation given by $i$=exp($i\pi/2$) must be altered. Clearly, if $\chi^{(3)}$ is complex, loss or gain of the field amplitude becomes possible, but this can be caused by material absorption (or gain) and not actual transfer of energy from the pump beam. In what follows we assume a purely refractive nonlinearity so that energy conservation in the light beams can be invoked. The question of whether or not energy is transferred between beams due to the grating produced by the interference between two beams is illustrated in Fig. 25. This figure is meant to give a physical picture of why the grating results in no net energy transfer if the phase of the grating is unshifted with respect to the irradiance modulation. The arrows point in the direction normal to the phase front (i.e. rays) and their size indicates the irradiance - for

equal input beams there is an equal irradiance in the direction of either beam, no net energy transfer. For unequal inputs, a little more thought shows that the initial imbalance is maintained. On the other hand, Figure 25 shows that a $\pi/2$ phase shift between the incident irradiance modulation and the material grating results in a net transfer of energy from one beam to the other (the direction depending on the sign of the phase shift). Deviation from a $\pi/2$ phase shift reduces the magnitude of the effect. The question remains of how to produce this phase shift.

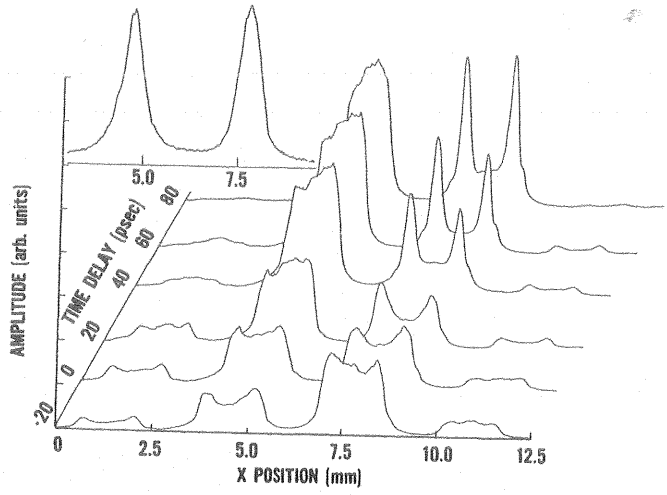


**Figure 24. The spatial profiles of equal energy "pump" and "probe" beams in the near field along with extra scattered beams at high irradiance as a function of the time delay between equal energy pump and probe beams (inset shows the pump and probe at low irradiance).**

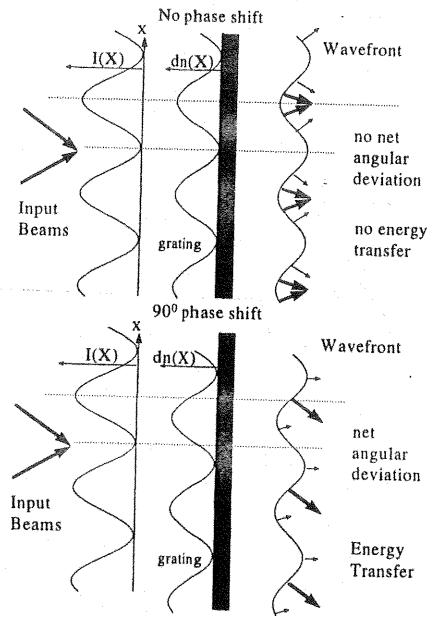


**Figure 25. An illustration of the physical reason for needing a $\pi/2$ phase shift between the interference pattern and the material refractive grating in order to have energy transfer.**

The photorefractive effect, utilizing charge migration and the electro-optic effect, is the usual example of how this phase shift is obtained.[40] In pulsed experiments the transient energy transfer that occurs from absorptive gratings leads to what are commonly referred to as coherent artifacts.[41,42] A phase shift is guaranteed for absorption gratings in the transient regime.[43,44,45,46] These coherent artifacts occur near zero temporal delay between the pulses (within the temporal coherence time) and transfer of energy from the stronger to the weaker beam. However, for purely refractive gratings, no energy transfer occurs even in the transient regime. In the example of silicon shown in Figs. 22-24 the nonlinearity was dominated by the refractive grating from the free-carriers. If, on the other hand, there is a frequency difference between the pump and probe, and the material response is non-instantaneous, a phase lag can occur between the refractive index grating and the moving irradiance interference pattern leading to energy transfer or 2-beam coupling. We give the following as an example of how the grating term can lead to energy transfer between beams for a purely refractive nonlinearity.

**Purely Refractive 2-Beam, Transient Energy Transfer**

Here the non-instantaneous nonlinearity is the optical Kerr effect due to reorientation of the cigar-shaped $CS_2$ molecules. The phase shift is produced by the phase lag of the material grating with respect to a moving interference pattern. The interference pattern is made to move by interfering two slightly different frequency beams. This results in transient energy transfer or two-beam coupling in $CS_2$ or other transparent Kerr liquids. The frequency difference results form using an initially chirped pulse which is split into pump and probe. The frequency difference then depends on the relative time delay between the two beams. Energy can be transferred from either beam to the other depending only on the relative delay (this changes the sign of the phase lag) with no transfer at zero time delay since then the grating is stationary (no frequency difference). Of course this scattering only occurs within the coherence time of the pulse (here picoseconds) where an interference grating is produced. Figure 26 shows the energy transfer as a function of time delay. This particular type of scattering is referred to as stimulated Rayleigh-wing scattering (SRWS). RWS is caused by thermal fluctuations of the macroscopic polarization due to fluctuations of the orientation of the individual dipoles. For these pulses the frequency increases with time in the pulse (i.e positive chirp). Thus, the first pulse always loses energy while the second pulse gains this energy.

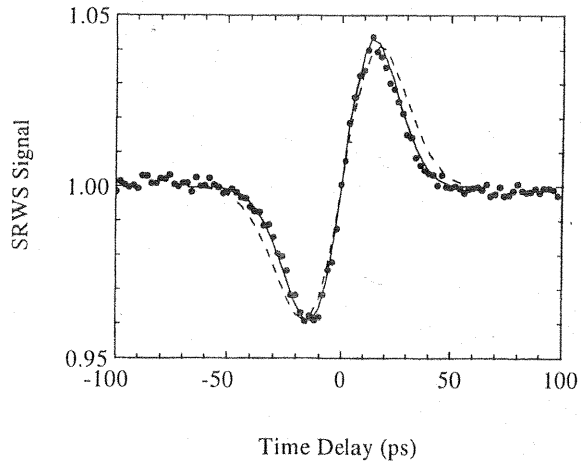


Figure 26. Energy transfer into and out of the probe beam as a function of time delay with respect to the pump beam (dashed line, theory for linear chirp - solid line, theory for actual chirp).

The only parameters needed for the theoretical fittings are the nonlinear index $n_2$, its relaxation time, $\tau$, and the linear chirp of the laser pulse. The first two are well known for $CS_2$ and the laser chirp can be independently measured using first and second order autocorrelation measurements. The chirp parameter, C, gives a measure of how rapidly the frequency changes per unit time within the pulse. Assuming a linear chirp the electric field is given by;

$$E(\vec{r},t) = E_0 \exp\left[i\left(\vec{k}\cdot\vec{r} - \omega t\right)\right]\exp\left[-\frac{1}{2}\left(\frac{t}{\tau_p}\right)^2(1+iC)\right], \tag{48}$$

where C is the linear chirp coefficient, and the coherence time is determined from $t_p = t_C\sqrt{1+C^2}$, where $\tau_p$ is the pulsewidth (HW1/eM). In this case we find the frequency difference, $\Omega$, between the two beams is linear in the time delay between pulses $\tau$, i.e. $\Omega = C\tau/\tau_p^2$. This leads to a simple expression for the signal, $S$;

$$S(\tau) = 1 + \frac{\Delta\Phi_0}{\sqrt{2}}\frac{\tau/t_m}{1+(\tau/t_m)^2}e^{-1/2(\tau/\tau_p)^2}, \tag{49}$$

where $t_m = \tau_p^2/C\tau_{rot}$, and $\tau_{rot}$ is the reorientation relaxation time. Even simpler, if the above expression is differentiated to find the peak and valley, the total change in transmittance between peak and valley, $\Delta T_{pv}$ (not related to a Z-scan) is

$$\Delta T = 2\sqrt{2}\exp(-1/2)\frac{\Delta\Phi_0 C\tau_{rot}}{\tau_p}, \tag{50}$$

where here $\Delta\Phi_0 = kn_2 I_{peak} L$. Figure 26 shows Eq. 49 fit to the signal obtained for $CS_2$.

Given the nonlinear refractive index, irradiance and chirp, the lifetime can be determined from this measurement. An interesting feature of the Eqs. 49 and 50 and the experiment on $CS_2$ is that lifetimes considerably shorter than the pulsewidth can be determined. In the case of $CS_2$, 24 ps (FWHM) pulses were used to measure a lifetime 10 times shorter, and the only limitation is how small a total change in transmittance can be measured. With high repetition rate femtosecond lasers using high frequency modulation methods $\Delta T_{pv}$ of $10^{-5}$ can be detected. With 100 fs pulses and $n_2$ values typical of transparent dielectrics, this should allow measurements of lifetimes of the order of 0.1 fs. This is of the estimated order of bound-electronic nonlinearities for these materials (so-called instantaneous nonlinearities).[47]

## ALL OPTICAL SWITCHING

An important application of the nonlinearities discussed in this chapter is switching use all-optical means (i.e. all-optical switching, AOS). The theory of $n_2$ and $\beta$ allows direct determination of the ideal operating point of a passive optical switch. Optical switch designers have established a figure-of-merit (FOM) for candidate materials, defined by the ratio $k_0 n_2/\beta$.[48] The goal of maximizing the FOM clearly shows the need for a large nonlinear phase shift ($\pi n_2/\lambda$) while keeping the 2PA loss ($\beta$) small. Using Eqs. 33 for $\beta$ and 36 for $n_2$, along with Eq. 37 relating the dispersion function G to F for 2PA, the FOM can be determined as shown in Fig. 27. Here the absolute value of the FOM is shown as the

solid line. Figure 27 also compares experimental data for several semiconductors to this theory. Note that the data here is the ratio of two experimental values, $\beta$ and $n_2$ for each material. The remarkable agreement between theory and experiment indicates that this quantity is indeed a fundamental property of semiconductors, depending only on the normalized optical frequency ($\hbar\omega/E_g$).

The two horizontal lines in Fig. 27 represent the minimum acceptable FOM for nonlinear directional couplers (NLDC) and Fabry-Perot (FP) interferometers. Although it demands a larger FOM, the NLDC scheme is the preferred practical geometry. From Fig. 27 we see that the FOM requirement is satisfied either just below the 2PA edge or very near resonance ($\hbar\omega \approx E_g$) . Since $n_2 \propto E_g^{-4}$, a low switching threshold at a given wavelength demands a material with the smallest possible bandgap energy. The theory then suggests that the ideal operating region is just below the bandgap. However, linear loss due to band-tail absorption makes this scheme unworkable at present. Operation near to but above the half bandgap where there is a small "resonance" in $n_2$ requires increased irradiance due to the reduced absolute magnitude of $n_2$, resulting in detrimental 2PA as discussed above. On the other hand, operation just below the $E_g/2$ eliminates 2PA with only a small reduction in $n_2$. It has recently been suggested that by using semiconductor laser amplifiers (SLA), parasitic linear loss can be mitigated, making near-gap operation a practical possibility.[49,50]

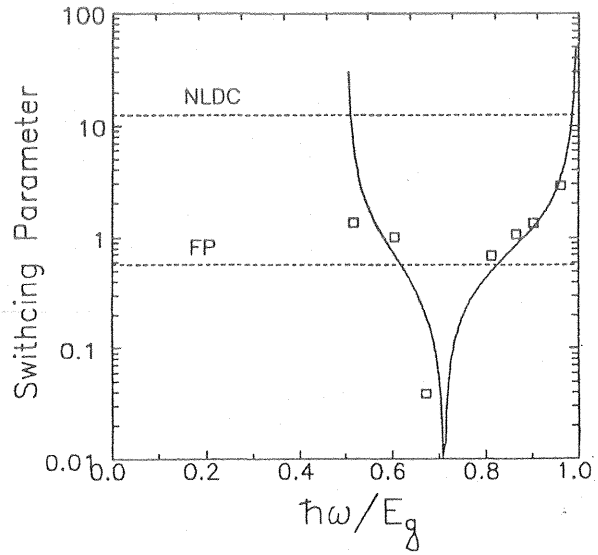


Fig. 27. All-optical switching figure of merit for passive optical switches. Adapted from Ref. 7.

## OPICAL LIMITING

Another application of the nonlinearities discussed above is for sensor protection against laser pulses. Devices for this purpose are called optical limiters. The ideal optical limiter has the characteristics shown in Fig. 28. It has a high linear transmission for low input (e.g. energy E or power P), a variable limiting input E or P, and a large dynamic range defined as the ratio of the E or P at which the device damages (irreversibly) to the limiting input. Such devices can also be used as power or energy regulators. However, since the primary application of the optical limiter is for sensor protection, and damage to detectors is almost always determined by fluence or irradiance, these are usually the quantities of interest for the output of the limiter. Getting the response of Fig. 28 turns out to be possible using a wide variety of materials; however, it is very difficult to get the limiting threshold as

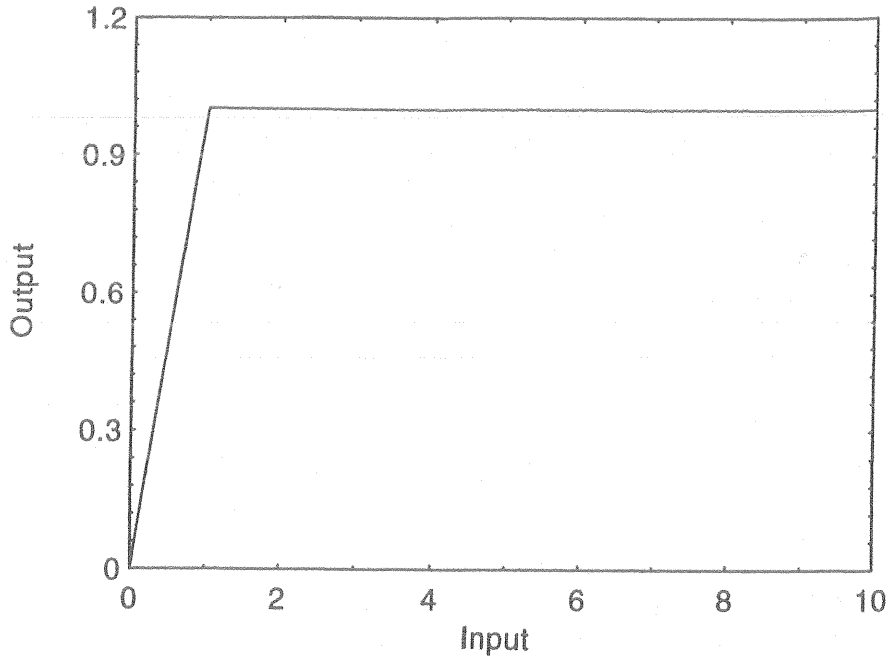


Figure 28. The ideal optical limiter input-output response characteristics.

low as is often required and at the same time have a large dynamic range. Because high transmission for low inputs is desired, we must have low linear absorption. These criteria lead to the use of two-photon absorption (2PA) and nonlinear refraction. Such devices work well for picosecond inputs. For example, a monolithic ZnSe device limits at inputs as low as 10 nJ (300 W), and has a dynamic range greater than $10^4$ for 0.53 μm, 30 ps (FWHM) pulses.[36] The liming effect from such a device is a combination of nonlinear loss from 2PA and free-carrier absorption and defocusing of the beam, which reduces the transmitted fluence, from free-carrier refraction. The lensing from $n_2$ is usually a smaller effect except when quite short pulses are used. Unfortunately, except in the IR, 2PA coefficients of inorganic solids are too small for most of these applications which look to protect against nanosecond sources. Organic materials have the potential for larger nonlinearities and are being actively investigated. In addition, if small linear absorption can be tolerated, reverse saturable absorbers can be effective.[51] Here the transmitted fluence is reduced so that the energy of a long pulse is limited as well as a short pulse as long as the pulsewidth is less than excited-state decay times.

## CONCLUSION

It should now be clear that the interpretation of NLA and NLR measurements is fraught with many pitfalls. Great care must be taken. In extensive studies of a wide variety of materials it is found that there is seldom a single nonlinear process occurring. Often several processes occur simultaneously, sometimes in unison, sometimes competing. For example we have given the example of potential confusion between "instantaneous" two-photon absorption and excited-state absorption. Such processes as reorientational, electrostrictive, thermal, saturation and excited-state nonlinearities can be thought of as two step processes, or cascaded $\chi^{(1)}:\chi^{(1)}$ nonlinearities. For example, for excited-state absorption, light first induces a transition creating an excited state (an $\mathrm{Im}\{\chi^{(1)}\}$ process) and then the excite state absorbs (a second $\mathrm{Im}\{\chi^{(1)}\}$ process), i.e., two linear absorption

processes. For these types of slow cumulative nonlinearities, the irradiance (or field) may no longer be the important input parameter. It makes sense to describe the ultrafast process of 2PA by $\chi^{(3)}$ or $\beta$ (sometimes $\alpha_2$ is also used in analogy to $n_2$) and the cumulative process of ESA or ESR by an absorptive or refractive cross section. Fourier transformation of the response function (see Eq. 1) results in the usually quoted frequency dependent susceptibility $\chi^{(n)}(\omega_1,\omega_2,\ldots,\omega_n)$. Memory, which was previously explicitly included in the response function, is lost in the dispersion. Thus, irradiance, I, and fluence, F, dependencies are treated equally. This can lead to confusion as the two processes (ultrafast and cumulative) are indistinguishable for pulses long compared to relevant relaxation processes. The usual expansion in terms of susceptibilities is useful for fast nonlinear responses but is often not the most convenient description and has been overused. Recently, studies of so-called $\chi^2{:}\chi^2$ cascading of second-order nonlinearitites have shown they can also mimic third-order responses of both $\beta$ and $n_2$.[52] It is necessary to experimentally distinguish and separate these various processes in order to understand and model the interactions. There are a variety of methods and techniques for determining the nonlinear optical response, each with its own weaknesses and advantages. In general, it is advisable to use as many complementary techniques as possible over a broad spectral range in order to unambiguously determine the active nonlinearities. Numerous techniques are known for measurements of NLR and NLA in condensed matter. Nonlinear interferometry, degenerate four-wave mixing (DFWM), nearly-degenerate three-wave mixing, ellipse rotation, beam distortion, beam deflection, and third-harmonic generation, are among the techniques frequently reported for direct or indirect determination of NLR. Z-scan is capable of separately measuring NLA and NLR. Other techniques for measuring NLA include transmittance, calorimetry, photoacoustic, and pump-probe methods.

## ACKNOWLEDGEMENT

I gratefully acknowledge the contributions of many of my colleagues, postdoctoral associates and graduate students, many of whom are included in the references. I also acknowledge the financial support of the National Science Foundation and DARPA over many years.

## REFERENCES

1. R. W. Boyd, *Nonlinear Optics*, Academic Press, Inc., 1992.
2. P. Meystre, and M. Sargent III, *Elements of Quantum Electronics*, 2nd ed., Springer Verlag, Berlin, 1991.
3. A.E. Kaplan, "External Self-focusing of Light by a Nonlinear Layer," Radiophys. Quantum Electron., 12, 692-696 (1969).
4. G.P. Agrawal, *Nonlinear Fiber Optics*, Academic Press, 1989.
5 J.S. Toll, "Causality and the dispersion relation: Logical Foundations", Phys. Rev. 104, 1760 (1956).
6. M. Sheik-Bahae, D.J. Hagan, and E.W. Van Stryland," Dispersion and Band-gap Scaling of the Electronic Kerr Effect in Solids associated with Two-Photon Absorption," Phys. Rev. Lett., 65, 96-99 (1989).
7. M. Sheik-Bahae, D.C. Hutchings, D.J. Hagan, and E.W. Van Stryland, "Dispersion of Bound-Electronic Nonlinear Refraction in Solids," IEEE J. Quantum Electron. QE-27, 1296-1309 (1991).
8. D.C. Hutchings, M. Sheik-Bahae, D.J. Hagan, E.W. Van Stryland, "Kramers-Kronig Dispersion Relations in Nonlinear Optics," Opt. Quantum Electron. , 24, 1-30 (1992).
9. F. Bassani and S. Scandolo, "Dispersion Relations in Nonlinear Optics", Phys. Rev., B44, 8446-53 (1991).
10. D.C. Hutchings and E.W. Van Stryland, "Nondegenerate two-photon absorption in zinc blende semiconductors," J. Opt. Soc. Am. B, B9, 2065-2074 (1992).
11. M. Sheik-Bahae, J. Wang and E.W. Van Stryland, "Nondegenerate Optical Kerr Effect in Semiconductors", IEEE. J. Quantum Electron, QE-30, 249-255 (1994).

12. E.W. Van Stryland, Arthur L. Smirl, Thomas F. Boggess, M.J. Soileau, B.S. Wherrett, and F. Hopf, "Weak-Wave Retardation and Phase-Conjugate Self-Defocusing in Si", in Picosecond Phenomena III, ed. K.B. Eisenthal, R.M. Hochstrasser, W. Kaiser, and A. Laubereau, Springer-Verlag, 368 (1982).
13. R.Y. Chiao, P. L. Kelley, and E. Garmire, Phys. Rev. Lett., 17, 1158 (1966).
14. J.A. Van Vechten and D.E. Aspnes, "Franz-Keldysh contribution to third-order optical susceptibilities" Phys. Lett., 30A, 346 (1969).
15. A. Yariv, "Quantum Electronics", 2nd Edn., Wiley, New York (1975).
16. R. Adair, L.L. Chase, and S.A. Payne, "Nonlinear Refractive Index of Optical Crystals", Phys. Rev. B, 39, 3337-3350 (1989).
17. Bechtel, J. H. and Smith, W. L., "Two-Photon Absorption in Semiconductors with Picosecond Laser Pulses", Phys. Rev. B, 13, 3515, (1976).
18. Eric W. Van Stryland, M.A. Woodall, H. Vanherzeele, and M.J. Soileau, "Energy Band-Gap Dependence of Two-Photon Absorption," Opt. Lett. 10, 490 (1985).
19. B.S. Wherrett, "Scaling Rules for Multiphoton Interband Absorption in Semiconductors", J. Opt. Soc. Amer., B1, 67 (1984).
20. H.S. Brandi and C.B. de Araujo, "Multiphoton Absorption Coefficients in Solids: a Universal Curve," J. Phys. C 16, 5929-5936(1983).
21. L.V. Keldysh, "Ionization in the field of a strong electromagnetic wave," Sov. Phys. JETP, 20, 1307-1314 (1965).
22. D.C. Hutchings and E.W. Van Stryland, "Nondegenerate two-photon absorption in zinc blende semiconductors," J. Opt. Soc. Am. B, B9, 2065-2074 (1992).
23. E. O. Kane, "Band structure of InSb", J. Chem. Phys. Solids, 1, 249 (1957).
24. P. Liu, W.L. Smith, H. Lotem, J.H. Bechtel, N. Bloembergen and R.S. Adhav, "Absolute Two-Photon Absorption Coefficients at 355 and 266 nm", Phys. Rev. B17, 4620 (1978).
25. Richard DeSalvo, A. Said, D. Hagan, and E. Van Stryland, "Infrared to Ultraviolet Measurements of 2-Photon Absorption and n2 in Wide Bandgap Solids", JQE QE-32, 1324-1333, (1996).
26. E. Van Stryland and L.L. Chase, "Two-Photon Absorption: inorganic materials", in Handbook of Laser Science and Technology; supplement 2: Optical Materials, section 8, pp. 299-326, Ed. M. Weber, CRC Press, 1994.
27. W. E. Williams, M. J. Soileau, and E. W. Van Stryland, "Simple direct measurement of n2", NBS Special pub. 688, 552-531, (1983).
28. M. Sheik-bahae, A.A. Said, and E.W. Van Stryland, "High Sensitivity, Single Beam n2 Measurements", Opt. Lett. 14, 955-957 (1989).
29. M. Sheik-bahae, A.A. Said, T.H. Wei, D.J. Hagan, and E.W. Van Stryland, "Sensitive Measurement of Optical Nonlinearities Using a Single Beam", Journal of Quantum Electronics, JQE, QE-26, 760-769 (1989).
30. T. Xia, D.J. Hagan, M. Sheik-Bahae, and E.W. Van Stryland, "Eclipsing Z-Scan Measurement of $\lambda/104$ Wavefront Distortion", Opt. Lett. 19, 317-319 (1994).
31. M. Sheik-Bahae, J. Wang, J.R. DeSalvo, D.J. Hagan and E.W. Van Stryland, "Measurement of Nondegenerate Nonlinearities using a 2-Color Z-Scan", Opt. Lett., 17, 258-260 (1992).
32. J. Wang, M. Sheik-Bahae, A.A. Said, D.J. Hagan, and E.W. Van Stryland, "Time-Resolved Z-Scan Measurements of Optical Nonlinearities", JOSA B11, 1009-1017 (1994).
33. R.K. Jain and M.B. Klein, "Degenerate Four-Wave Mixing in Semiconductors", pp. 307-415, in Optical Phase Conjugation, ed. R. A. Fisher, Academic Press, N.Y. 1983.
34. Optical Phase Conjugation, ed. R. A. Fisher, Academic Press, N.Y. 1983.
35. E. Canto-Said, D. J. Hagan, J. Young, and E. W. Van Stryland, "Degenerate Four-Wave Mixing Measurements of High Order Nonlinearities in Semiconductors", IEEE J. Quantum Electron. 27, 2274 (1991).
36. E.W. Van Stryland, Y.Y. Wu, D.J. Hagan, M.J. Soileau, and Kamjou Mansour, "Optical Limiting with Semiconductors," JOSA B5, 1980-89, (1988).
37. A. A. Said, M. Sheik-Bahae, D.J. Hagan, T. H. Wei, J. Wang, J. Young, and E. W. Van Stryland, "Determination of Bound-Electronic and Free-Carrier Nonlinearities in ZnSe, GaAs, CdTe, and ZnTe", J. Opt. Soc. Am., B9, 405 (1992).
38. T. H. Wei, D. J. Hagan, E. W. Van Stryland, J, W. Perry, and D. R. Coulter, "Direct Measurements of Nonlinear Absorption and Refraction in Solutions of Pthalocyanines", Appl. Phys. B54, 46 (1992).
39. C.R. Giuliano and L. D. Hess, "Nonlninear Absorption of Light: Optical Saturation of Electronic Transitions in Organic Molecules with High Intensity Laser Radiation", IEEE J. Quant. Electron. QE-3, 338-367 (1967).
40. Photorefractive Materials and Their Applications, Topics in Applied Optics, Vol. 61, Eds. P. Gunter and J.P. Huignard, Springer Verlag, Berlin, 1988.

41. E. P. Ippen and C. V. Shank, in Ultrashort Light Pulses, S. L. Shapiro, ed., Vol. 18 of Topics in Applied Physics, p. 83, Springer-Verlag, Berlin, 1977.
42. Z. Vardeny and J. Tauc, "Picosecond coherence coupling in the pump and probe technique," Opt. Commun. 39, 396 (1981).
43. P. S. Spencer and K. A. Shore, "Pump-probe propagation in a passive Kerr nonlinear optical medium," J. Opt. Soc. Am. B 12, No. 1, 67 (1995).
44. K. D. Dorkenoo, D. Wang, N. P. Xuan, J. P. Lecoq, R. Chevalier and G. Rivoire, "Stimulated Rayleigh-wing scattering with two-beam coupling in CS2," J. Opt. Soc. Am. B 12, No. 1, 37 (1995).
45. G. Rivoire and D. Wang, "Dynamics of CS2 in the large spectral bandwidth stimulated Rayleigh-wing scattering," J. Chem. Phys. 99, No. 12, 9460 (1993).
46. R. Y. Chiao and J. Godine, "Polarization dependence of stimulated Rayleigh-wing scattering and the optical-frequency Kerr effect," Phys. Rev. 185, No. 2, 430 (1969).
47. Arthur Dogariu and David J. Hagan, "Low frequency Raman gain measurements using chirped pulses", Optics Express, 1, 73 (1997).
48. G.I. Stegeman, E.M. Wright, "All-optical waveguide switching," Optical and Quantum Electronics, 22, 95-122 (1990).
49. C.T. Haltgren, E.P. Ippen, "Ultrafast refractive index dynamics in AlGaAs diode laser amplifiers," Appl. Phys. Lett. 59, 635-638 ((19991).
50. K. L. Hall, G. Lenz, , E.P. Ippen, G. Raybon, "Heterodyne pump-probe technique for time-domain studies of optical nonlinearities in waveguides," Opt. Lett. 17, 874-877 (1992).
51. D.J. Hagan, T. Xia, A.A. Said, T.H. Wei, and E.W. Van Stryland, "High Dynamic Range Passive Optical Limiters", International Journal of Nonlinear Optical Physics vol. 2, 483-501 (1993).
52. R.J. DeSalvo, D.J. Hagan, M. Sheik-Bahae, G. Stegeman, H. Vanherzeele and E.W. Van Stryland, "Self-Focusing and Defocusing by Cascaded Second Order Effects in KTP", Opt. Lett. 17, 28 (1991).